



1 **Air–sea CO<sub>2</sub> exchange in the Southern Adriatic Sea: assessing**  
2 **its role as a moderate carbon sink over the last decade**

3 Carlotta Dentico<sup>1,2</sup>, Gianpiero Cossarini<sup>2</sup>, Giuseppe Civitarese<sup>2</sup>, Michele Giani<sup>2</sup>, Angelo Rubino<sup>1</sup> and Vanessa  
4 Cardin<sup>2</sup>

5

6 <sup>1</sup> Department of Environmental Sciences, Informatics and Statistics, Università Cà Foscari, Venice, Italy

7 <sup>2</sup> National Institute of Oceanography and Applied Geophysics (OGS), Trieste, Italy

8

9 *Correspondence to:* Carlotta Dentico ([cdentico@ogs.it](mailto:cdentico@ogs.it))

10

11

**Abstract**

12 Coastal waters contribute significantly to the total oceanic carbon uptake. In this context, the cumulative  
13 influence exerted by marginal seas may be conspicuous. However sparse and unevenly distributed  
14 observations in such regions pose a serious limit to an accurate, experimentally based quantification of  
15 carbon dynamics. The Southern Adriatic (SAd) is one of the key sites of the Mediterranean Sea where  
16 open-ocean deep water formation occurs, a process recognized as a major driver of carbon  
17 sequestration. However, only a limited number of studies have investigated surface carbon dynamics  
18 and quantified air-sea carbon flux in the SAd. In this study, a newly validated, decade-long (2015-2024)  
19 high-resolution time series of CO<sub>2</sub> and hydrographic measurements collected at the EMSO-E2M3A  
20 South Adriatic observatory, located at the center of the Southern Adriatic Pit, has been analysed. The  
21 results showed that seasonal temperature variability and winter convection were the main processes  
22 driving the dynamics of surface partial pressure of CO<sub>2</sub> ( $p\text{CO}_{2\text{sw}}$ ). Air–sea CO<sub>2</sub> flux (FCO<sub>2</sub>), derived  
23 from in situ observations, indicated a clear seasonal pattern, with the SAd acting as a CO<sub>2</sub> sink during  
24 winter and as a source during summer. Importantly, the results revealed that the SAd acted as a moderate  
25 carbon sink over the last decade. Uncertainty analysis in the flux estimates were also evaluated,  
26 revealing that wind speed input data used for FCO<sub>2</sub> calculations influenced the magnitude of FCO<sub>2</sub>.  
27 Finally, the results presented here showed how time series such as the SAd dataset can serve as critical  
28 assets for validating operational ocean models, such as the EU Copernicus Marine Service for the  
29 Mediterranean, by helping to identify discrepancies in the simulation of key processes.

30

**1. Introduction**

31 In the decade 2014-2023 it is estimated that the ocean has absorbed 10.5 GtCO<sub>2</sub> on average each year,  
32 which corresponds to around 26% of total CO<sub>2</sub> emissions (Friedlingstein et al., 2025). The concentration  
33 of carbon dioxide (CO<sub>2</sub>) in the atmosphere has increased from approximately 278 parts per million  
34 (ppm) at the beginning of the Industrial Revolution (Gulev et al., 2021), to more than 421 ppm at the  
35 end of 2024 (Lan et al., 2024). This has led to an increasing ocean carbon uptake, which, in turn, has



36 caused changes in seawater chemistry. The exchange of CO<sub>2</sub> across the air-sea interface is driven by  
37 the difference between the partial pressure of CO<sub>2</sub> in the seawater ( $p\text{CO}_{2\text{sw}}$ ) and in the atmosphere  
38 ( $p\text{CO}_{2\text{atm}}$ ). The CO<sub>2</sub> absorbed by the ocean reacts with seawater to form carbonic acid (H<sub>2</sub>CO<sub>3</sub>), much  
39 of which dissociates releasing hydrogen ions (H<sup>+</sup>), bicarbonate (HCO<sub>3</sub><sup>-</sup>), and, to a lesser extent,  
40 carbonate ions (CO<sub>3</sub><sup>2-</sup>) according to the salinity, pressure and temperature dependent equilibrium  
41 constants (Zeebe & Wolf-Gladrow, 2001). The increased concentration of hydrogen ions causes a  
42 reduction of pH and of carbonate ions in seawater. This process is commonly referred to as ocean  
43 acidification (Doney et al., 2009; Gattuso and Hansson, 2011) and is one of the major threats to many  
44 marine organisms. Carbonate ions are an important building block of structures such as sea shells and  
45 coral skeletons. Decreases in carbonate ions can make building and maintaining shells and other calcium  
46 carbonate structures more difficult for calcifying organisms such as shellfish, corals and calcareous  
47 plankton (e.g., Ilyina et al., 2009; Lohbeck et al., 2012; Meyer and Riebesell, 2015) putting on risk the  
48 entire food web.

49 Global estimates of ocean carbon flux rely on both observations and models (Gruber et al., 2023;  
50 Friedlingstein et al., 2025). Many efforts have been made by the scientific community to increase the  
51 number and availability of carbon measurements from different sources (e.g., from research vessels,  
52 autonomous sensors, Argo floats) into quality controlled and openly accessible data products, resulting  
53 in more than 30 million observations in the Surface Ocean CO<sub>2</sub> Atlas (SOCAT) V2022 release.  
54 However, these observations cover only a small fraction of the ocean surface and the amount of new  
55 observations per year in the open ocean has decreased since 2017 (Bakker et al., 2023). Ocean  
56 reanalyses have demonstrated significant potential in bridging observational gaps by providing  
57 comprehensive, three-dimensional, basin-wide datasets that enable the investigation of spatial and  
58 temporal variability across multiple scales (Cossarini et al., 2021). However, generating a coupled  
59 physical-biogeochemical reanalysis remains a complex challenge (Park et al., 2018), due to  
60 uncertainties in the representation of interactions between physical and biogeochemical processes, the  
61 limited availability of biogeochemical observations for both data assimilation and validation, and the  
62 multivariate nature of the biogeochemical system, which involves intricate relationships between  
63 observed and modeled variables (Cossarini et al., 2021). As a result, models still struggle to accurately  
64 represent sparsely sampled regions, and considerable uncertainties persist, particularly in marginal and  
65 coastal seas (Resplandy et al., 2024). Despite their small size (about 7% of the global ocean area),  
66 marginal and coastal seas have a significant impact on the carbon cycle (Lee et al., 2011; Kapsenberg  
67 et al., 2017; Laruelle et al., 2018; Hassoun et al., 2019; Resplandy et al., 2024). The latest estimates  
68 from Roobaert et al. (2024) quantified the global coastal CO<sub>2</sub> flux equal to -2.2 GtCO<sub>2</sub> yr<sup>-1</sup> (-0.6 PgC  
69 yr<sup>-1</sup>) which represent around 21% of the total current CO<sub>2</sub> flux from the atmosphere to the ocean (10.5  
70 GtCO<sub>2</sub>; Friedlingstein et al., 2025). The seawater carbonate system in these regions is driven by complex  
71 interaction between physical and chemical processes, like the overturning circulation, ocean mixing,



72 freshwater inputs and biological processes. These interactions vary over time and space highlighting  
73 the importance of sustained time series observations to better understand and separate their individual  
74 contributions (Garcia-Ibañez et al., 2024). Thus, in situ observations are of paramount importance to  
75 provide high spatiotemporal resolution in specific areas of interest, to monitor Essential Ocean  
76 Variables (EOVs), to inform about ocean conditions throughout the water column (Schroeder et al.,  
77 2022) and to assess the quality of different model products and satellite measurements.

78 The Mediterranean Sea is a semi-enclosed basin, where Atlantic Ocean water is exchanged through the  
79 Strait of Gibraltar and is one of the areas where CO<sub>2</sub> estimations remain sparse and unevenly distributed  
80 (Hassoun et al., 2022). Here, two major overturning circulation cells contribute to transporting carbon  
81 from the surface to the ocean interior (Lee et al., 2011). In the eastern Mediterranean, the northern and  
82 southern Adriatic play a key role in sustaining the thermohaline circulation (Robinson et al., 2001) and  
83 in capturing and storing CO<sub>2</sub> in the deeper layers (Cantoni et al., 2016; Ingrosso et al., 2017; Urbini et  
84 al., 2020; Cantoni et al., 2024). In particular, the Northern Adriatic Deep Water (NAAdW) represents  
85 the densest and most CO<sub>2</sub>-rich water mass in the region, significantly contributing to deep ventilation  
86 and carbon sequestration in the eastern Mediterranean basin.

87 In this study, a new validated in situ time series of sea surface observations from the EMSO-E2M3A  
88 South Adriatic regional facility and ICOS ERIC observatory (nominal position 41.5053°N, 18.0806°E),  
89 hereafter EMSO-E2M3A, is presented. Time series of sea water partial pressure of CO<sub>2</sub> ( $p\text{CO}_{2\text{sw}}$ ,  $\mu\text{atm}$ ),  
90 hydrography and estimated CO<sub>2</sub> flux ( $\text{FCO}_2$ ,  $\text{mmol m}^{-2} \text{day}^{-1}$ ) are discussed. One of the major goals of  
91 this research is to assess the role of the southern Adriatic (SAd) as a carbon sink or source in the last  
92 decade. To our knowledge, this is the first time that a comprehensive study on carbon dynamics and  
93 carbon flux in the region using high resolution in situ observations has been achieved. Further, it is  
94 shown how the SAd  $p\text{CO}_{2\text{sw}}$  and  $\text{FCO}_2$  time series can be a key asset for biogeochemical reanalyses.  
95 Considering the Mediterranean Copernicus Marine Service biogeochemical reanalysis, the SAd data  
96 allowed to validate the biogeochemical reanalyses as a good tool to represent local dynamics while  
97 highlighting the presence of some differences in the amplitude of seasonal cycles of both  $p\text{CO}_{2\text{sw}}$  and  
98  $\text{FCO}_2$ .

99 The paper is organized as follows. Section 2 describes the study area, Section 3 describes the data used  
100 and the thermodynamic calculation performed to estimate carbon flux. Results are presented and  
101 discussed in section 4. Conclusions are provided in Section 5.

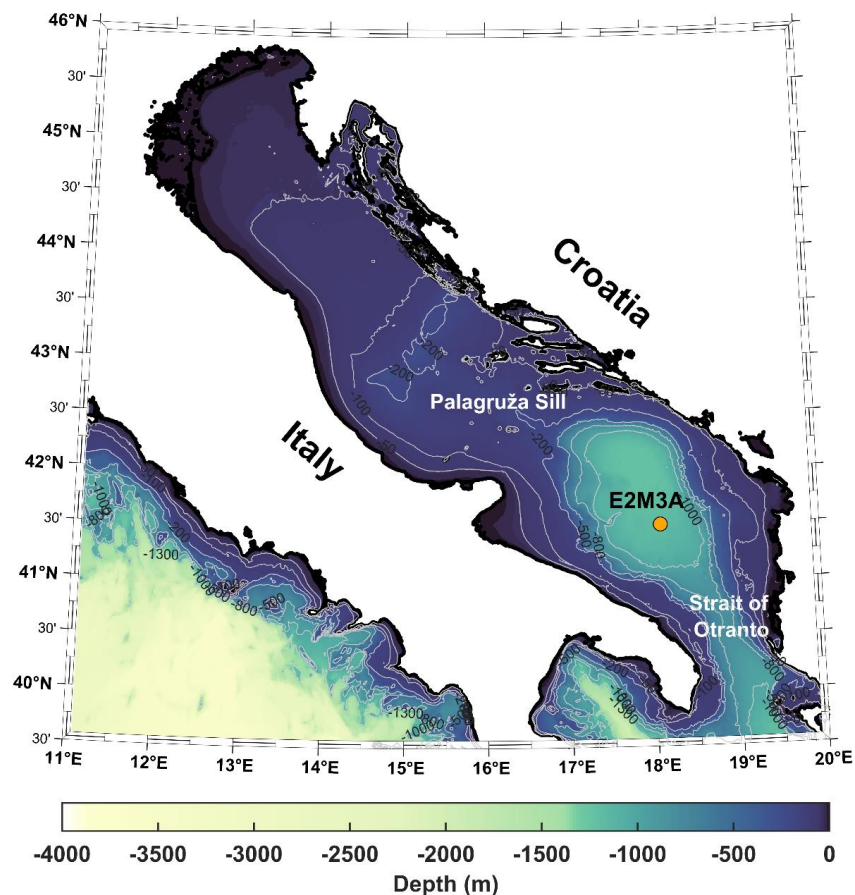
102

## 103 2. Study area

104 The southern Adriatic (SAd) is located between the Palagruža Sill and the Strait of Otranto, where  
105 maximum depth reaches about 1250 m in the Southern Adriatic Pit (SAP; Figure 1). This area is featured  
106 by a quasi-permanent cyclonic circulation, and it is well known that dense water formation takes place  
107 at the centre of the gyre through open-ocean convection (Ovchinnikov et al., 1985; Gačić et al., 2002;

108 Mantziafou and Lascaratos, 2004; Chiggiato et al., 2016; Amitai et al., 2021) contributing to the eastern  
109 Mediterranean thermohaline circulation (Robinson et al., 2001).

110



111

112 **Figure 1.** Map of the study area. The location of EMSO-E2M3A (nominal position 41.5053°N,  
113 18.0806°E) moored at the center of the SAP is shown by the orange dot. The geographical boundaries  
114 of the southern Adriatic, i.e., the Palagruža Sill and the Strait of Otranto, are also displayed and  
115 highlighted by the two red lines.

116

117 The variability of physical and biogeochemical processes, including ocean carbon dynamics, is related  
118 to the interaction of different water masses (Civitarese et al., 2023). The Adriatic Dense Water (AdDW)  
119 occupies the bottom layer of the SAP and represents the main component of dense water for the whole  
120 Eastern Mediterranean basin (Schlitzer et al., 1991; Roether and Schlitzer, 1991). About 82 % of this  
121 water mass is formed through winter convection in the SAd (Ingrosso et al., 2017), while the remaining  
122 part has its origin on the northern Adriatic shelf and in the middle Adriatic Sea (Ovchinnikov et al.,



123 1985; Bignami et al., 1990; Malanotte-Rizzoli, 1991). The Northern Adriatic Dense Water (NAdDW)  
124 is formed in the shallow northern Adriatic during winter, due to the cooling of the entire water column  
125 and of the evaporation caused by E-NE wind (named Bora). The process of formation of NAdDW is  
126 characterised by a high interannual variability as it is preconditioned by periods of low freshwater  
127 discharge by the rivers at least 4-5 months before its generation (Vilibić and Supić, 2005). These  
128 meteorological and oceanographic conditions also favour CO<sub>2</sub> and O<sub>2</sub> dissolution when surface water  
129 is undersaturated with respect to the overlying atmosphere. The CO<sub>2</sub> and oxygen enriched NAdDW is  
130 usually partially filling the middle Adriatic Pit and partly flows southward to the SAP (Cardin et al.,  
131 2011). On an interannual time scale, the physical and biogeochemical dynamics of the SAd is also  
132 strictly linked to that of the Ionian Sea (IS) by means of the Bimodal Oscillating System (BiOS). This  
133 mechanism changes the vorticity of the North Ionian Gyre (NIG) from cyclonic to anticyclonic and vice  
134 versa (Gačić et al., 2010; Civitarese et al., 2010; Civitarese et al., 2023). When the NIG is anticyclonic,  
135 the Modified Atlantic Water (MAW) coming from the Sicily Channel is in part deviated toward the  
136 northern Ionian and eventually enters the SAd, decreasing the salinity and the density of the AdDW.  
137 The change in the properties of the outflowing AdDW causes a progressive weakening of the  
138 anticyclonic upper-layer circulation in the IS. The circulation reverses, modifying the pathways of the  
139 water masses suppressing the northern branch of the MAW flow and favours the rapid advection of  
140 salty Levantine and/or Cretan Intermediate Water (LIW; CIW) along the eastern flank of the IS into the  
141 SAd. This results in an increase in the salinity (and density) of AdDW outflowing into the IS that  
142 gradually impairs the cyclonic NIG, eventually reversing it to an anticyclone. Finally, along the western  
143 coast in the SAd, the Adriatic Surface Water (AdSW) can be found. This is a relatively fresh and warm  
144 water mass, which originates from the northern Adriatic rivers runoff and flows southward along a  
145 narrow coastal layer of the western Italian shelf and exits through the Strait of Otranto.

146 The variability of the biogeochemical properties and the carbonate system of the SAd were almost  
147 continuously monitored by open ocean observatories, sampling activities and by ocean Argo floats and  
148 gliders. Particularly, the EMSO-E2M3A, which is located at the center of the SAP (Figure 1) and it is  
149 operated by the Italian National Institute of Oceanography and Applied Geophysics (OGS), represents  
150 a key research infrastructure to study biogeochemical and hydrographical properties of the whole water  
151 column in the SAP. EMSO-E2M3A is part of the European Multidisciplinary Seafloor and water  
152 column Observatory (EMSO) and the ICOS (Integrated Carbon Observation System) ERIC networks.  
153 It consists of a system of two moorings, with the main mooring housing the surface buoy and it is  
154 equipped with a meteorological station and radiometers, sensors for physical (hydrography) and  
155 chemical variables ( $p\text{CO}_{2\text{sw}}$ , dissolved oxygen and pH), telemetry and services (Ravaioli et al., 2016).  
156 The secondary mooring line is composed of an instrument chain with sensors at different depths for  
157 physical and chemical measurements from the seafloor to the intermediate layer (Cardin et al., 2025a).  
158 The station has been in operation almost continuously since 2006 and is the longest open sea time series  
159 in the Adriatic.



160

### 161 3. Data and Methods

#### 162 3.1. In situ measurements

163 The time series of  $p\text{CO}_{2\text{sw}}$  and hydrological variables presented in this study were measured by different  
164 sensors at the EMSO-E2M3A (Cardin et al., 2025b). A ProOceanus  $\text{CO}_2$  sensor provided autonomous  
165 high-frequency (every four hours) measurements of  $p\text{CO}_{2\text{sw}}$  ( $\mu\text{atm}$ ) from 2015 to 2024 with declared  
166 accuracy of  $\pm 5 \mu\text{atm}$ . Hourly sea surface temperature (SST,  $^\circ\text{C}$ ), salinity (Sal) and dissolved oxygen  
167 (DO,  $\mu\text{mol kg}^{-1}$ ) were measured by a SeaBird SBE 37-ODO with declared accuracy of  $\pm 0.002 \text{ }^\circ\text{C}$ ,  $\pm$   
168  $0.003 \text{ mS cm}^{-1}$ ,  $\pm 0.1 \%$  full scale range, respectively. DO from SBE 37-ODO was also used to calculate  
169 the apparent oxygen utilization (AOU,  $\mu\text{mol kg}^{-1}$ ). This value corresponds to the difference between the  
170 equilibrium saturation of oxygen concentration in seawater with the same physical and chemical  
171 properties and the measured oxygen concentration, providing an estimation of the balance between  
172 primary production and respiration. AOU has been computed using the solubility coefficients from  
173 Benson and Krause (1984) as fitted by Garcia and Gordon (1992). A detailed description of the dataset  
174 used here and the quality control procedures applied to the data are available in Dentico et al. (2025).  
175 To calculate air-sea  $\text{FCO}_2$ , hourly atmospheric molar fraction of  $\text{CO}_2$  ( $x\text{CO}_2$ , ppm) from the ENEA  
176 Station for Climate Observations on the island of Lampedusa (Marullo et al., 2021; di Sarra et al., 2025)  
177 were used. Indeed, atmospheric  $p\text{CO}_2$  measurements ( $p\text{CO}_{2\text{atm}}$ ,  $\mu\text{atm}$ ) at EMSO-E2M3A only started in  
178 December 2023, when a ProOceanus  $\text{CO}_2$ -Pro ATM was deployed allowing continuous measurements  
179 of both  $p\text{CO}_{2\text{sw}}$  and  $p\text{CO}_{2\text{atm}}$  in alternating mode. As in situ observations of  $p\text{CO}_{2\text{atm}}$  were not long  
180 enough to match with  $p\text{CO}_{2\text{sw}}$ , Lampedusa data was chosen as it represents one of the longest oceanic  
181 time series of  $p\text{CO}_{2\text{atm}}$  in the Mediterranean sea. Moreover, these data have been used in similar studies  
182 to compute  $\text{FCO}_2$  at Mediterranean scale (e.g., Martellucci et al., 2024a; 2025) and in the northern  
183 Adriatic Sea (e.g., Urbini et al., 2020; Cantoni et al., 2024). From Lampedusa  $x\text{CO}_2$  (indicated as  
184  $x\text{CO}_{2\_LMP}$ ), the  $p\text{CO}_{2\text{atm}}$  relative to the local physical and atmospheric condition at EMSO-E2M3A  
185 (indicated as  $p\text{CO}_{2\text{atm\_E2M3Ar}}$ ) was calculated according to Weiss et al., (1974):

186

$$187 \quad p\text{CO}_{2\text{atm\_E2M3Ar}} = x\text{CO}_{2\_LMP} (P - p\text{H}_2\text{O}) \quad (1)$$

188

189 where  $P$  is the air pressure (mbar) measured at EMSO-E2M3A and  $p\text{H}_2\text{O}$  (mbar) is the water vapour  
190 saturation that has been calculated according to Weiss and Price (1980):

191

$$192 \quad p\text{H}_2\text{O} = A \exp^{(B - C(100/SST) - D \log(SST/100) - E(SSS))} \blacksquare \quad (2)$$

193

194 where  $SST$  is sea surface temperature (K),  $SSS$  is sea surface salinity both measured at EMSO-E2M3A  
195 and the coefficients  $A$ ,  $B$ ,  $C$  and  $D$  can be found in Weiss and Price (1980). To assess the potential bias



196 of using  $x\text{CO}_2_{\text{LMP}}$  for the calculation of  $\text{CO}_2$  air-sea flux in the SAd, a comparison between  $p\text{CO}_{2\text{atm}}$   
197 measured by the ProOceanus  $\text{CO}_2$ -Pro ATM sensor installed at EMSO-E2M3A ( $p\text{CO}_{2\text{atm\_E2M3A}}$ ) with  
198  $p\text{CO}_{2\text{atm\_E2M3Ar}}$  was performed. This comparison was limited to a four-month period between December  
199 2023 and March 2024, when the  $\text{CO}_2$ -Pro ATM sensor was operational. The two time series show good  
200 overall agreement, however the differences tend to be larger at higher  $p\text{CO}_{2\text{atm}}$  values, while they remain  
201 smaller at lower values (Fig. S1, S2a, Supplementary Material). A mean difference of  $+2.67 \pm 3.15$   
202  $\mu\text{atm}$  between  $p\text{CO}_{2\text{atm\_E2M3A}}$  and  $p\text{CO}_{2\text{atm\_E2M3Ar}}$  indicate that  $p\text{CO}_{2\text{atm\_E2M3A}}$  is on average higher than  
203  $p\text{CO}_{2\text{atm}}$  derived from  $x\text{CO}_2_{\text{LMP}}$ . A detailed investigation of the reasons behind this difference was  
204 beyond the scope of this work. Although the analysis of the residuals indicated potential  
205 heteroscedasticity in the data (Fig. S2a, S2b, Supplementary Material), the short duration of the  
206 overlapping time series justified applying a constant bias correction of  $+2.67 \mu\text{atm}$  to  $p\text{CO}_{2\text{atm\_E2M3Ar}}$ .  
207 To evaluate the robustness of this correction, a comparison between  $p\text{CO}_{2\text{atm}}$  derived from the CAMS  
208 reanalysis of the European Centre for Medium-Range Weather Forecasts (ECMWF; Agustí-Panareda  
209 et al., 2023), was also considered (Figure S3, Supplementary Material). The difference between monthly  
210  $p\text{CO}_{2\text{atm}}$  data at Lampedusa (LMP) and at EMSO-E2M3A between 2003 and 2021 was 2 ppm which is  
211 similar to the offset estimated in the four-month period. Finally, wind speed (WSPD,  $\text{m s}^{-1}$ ) was  
212 measured by a Young sensor on the meteorological station at EMSO-E2M3A (Cardin et al., 2025b;  
213 Dentico et al., 2025) with a manufacturer accuracy of  $\pm 0.3 \text{ m s}^{-1}$  and was used as input for  $\text{CO}_2$  flux  
214 calculation. Given that at EMSO-E2M3A wind speed is measured at 2 m height and  $\text{CO}_2$  air-sea flux  
215 calculation requires the standard reference height of 10 m (Wanninkhof, 2014), a conversion was  
216 performed using a logarithm wind speed profile according to:

217

$$218 \quad u_{\text{LOG}(z)} = (\ln(z/z_0) / \ln(z_m/z_0))u_{(z_m)} \quad (3)$$

219

220 where  $u_{\text{LOG}(z)}$  is the wind speed ( $\text{m s}^{-1}$ ) at the desired height (10 m),  $z$  is the desired measurement  
221 height (10 m),  $z_m$  the actual measurement height (2 m),  $z_0$  is the roughness length that for oceanic  
222 regions was set equal to  $1.52 \times 10^{-4}$  (Peixoto and Ort, 1992) and  $u_{(z_m)}$  is the wind speed ( $\text{m s}^{-1}$ ) measured  
223 at EMSO-E2M3A at 2 m height.

224

### 225 3.2. Model data

226 The EU Copernicus Marine Service (CMEMS) provides regular and systematic information on the  
227 ocean physics and biogeochemistry for the global ocean and the European regional seas (Le Treon et  
228 al. 2019). Data from different Mediterranean CMEMS products were used as an additional reference to  
229 investigate the variability of the in situ  $p\text{CO}_{2\text{sw}}$  and  $\text{FCO}_2$ . In particular, the following modelling  
230 products were used: the Sea Physics Reanalysis (PHY, Escudier et al., 2021) for the physical variables  
231 of surface temperature (SST,  $^{\circ}\text{C}$ ), salinity (Sal) and Mixed Layer Depth (MLD, m), the Biogeochemistry



232 Reanalysis (RD; Cossarini et al., 2021) and the Biogeochemistry Analysis and Forecast product (AF;  
 233 Salon et al., 2019) for  $p\text{CO}_{2\text{sw}}$  ( $\mu\text{amt}$ ) and  $\text{FCO}_2$  ( $\text{mmol m}^{-2} \text{day}^{-1}$ ). Additionally, the Ocean Color  
 234 Satellite product (Volpe et al., 2019) of the surface chlorophyll-a (Chl-a,  $\mu\text{g l}^{-1}$ ) was used as a proxy of  
 235 primary production. Detailed information on the models and variables used are summarized in Table 1.  
 236 The time series presented here are spatial averages of the grid points in the 10 km radius from EMSO-  
 237 E2M3A from the native spatial resolution of 4.5 km and 1 km for models and satellite data, respectively.  
 238

239 **Table 1.** Overview of the Copernicus Marine Service (CMEMS) products used in this work.

CMEMS product name	Variables used in this work	DOI	Reference
Mediterranean Sea Physics Reanalysis (PHY)	SST, Sal, MLD	<a href="https://doi.org/10.25423/CMCC/MEDSEA_MULTIYE_AR_PHY_006_004">https://doi.org/10.25423/CMCC/MEDSEA_MULTIYE_AR_PHY_006_004</a>	Escudier et al., (2021)
Mediterranean Sea Biogeochemistry Reanalysis (RD)	$p\text{CO}_{2\text{sw}}$ , $\text{FCO}_2$	<a href="https://doi.org/10.25423/cmcc/medsea_multiyear_bgc_006_008_medbfm3">https://doi.org/10.25423/cmcc/medsea_multiyear_bgc_006_008_medbfm3</a>	Cossarini et al., (2021)
Mediterranean Sea Biogeochemistry Analysis and Forecast (AF)	$p\text{CO}_{2\text{sw}}$ , $\text{FCO}_2$	<a href="https://doi.org/10.25423/cmcc/medsea_analysisforecast_bgc_006_014_medbfm4">https://doi.org/10.25423/cmcc/medsea_analysisforecast_bgc_006_014_medbfm4</a>	Salon et al., (2019)
Mediterranean Sea, Bio-Geo-Chemical, L4, monthly means, daily gapfree and climatology Satellite Observations (1997-ongoing)	Chl-a	<a href="https://doi.org/10.48670/moi-00300">https://doi.org/10.48670/moi-00300</a>	Volpe et al., (2019)

240

241 ERA5 wind product, which is the fifth generation of ECMWF reanalysis for the global climate and  
 242 weather (Hersbach et al., 2023), was also used and compared with EMSO-E2M3A wind measurements.  
 243 ERA5 provides hourly estimates for a large number of atmospheric, ocean-wave and land-surface  
 244 quantities from 1940 to present. The spatial resolution of atmospheric data is  $0.25^\circ \times 0.25^\circ$  and wind  
 245 speed ( $\text{WSPD}_{\text{ERA5}}$ ,  $\text{m s}^{-1}$ ) in the subregion close to EMSO-E2M3A (30 km radius) was calculated  
 246 according to the following:

247

$$248 \text{WSPD}_{\text{ERA5}} = \sqrt{u^2 + v^2} \quad (4)$$

249



250 where  $u^2$  is the square of the 10 m u-component ( $\text{m s}^{-1}$ ), which is the eastward horizontal wind speed,  
251 while  $v^2$  is the square of the 10 m v-component ( $\text{m s}^{-1}$ ) that represents the northward horizontal wind  
252 speed. ERA5 wind speed data were selected for two main reasons: (i) wind reanalysis products, unlike  
253 in situ time series, provide continuous spatial and temporal coverage without observational gaps; (ii)  
254 ERA5 wind data are used as the wind forcing input in the Mediterranean Sea Physical and  
255 Biogeochemistry Reanalyses. Thus, considering that  $\text{CO}_2$  air-sea flux in the CMEMS products and in  
256 the present work was computed following the same formulation (Wanninkhof, 2014), the use of the  
257 same wind dataset, allowed a focus on the analyses of  $p\text{CO}_{2\text{sw}}$  difference between in situ data and model  
258 outputs. Nevertheless, a validation of the ERA5 wind data using local wind conditions at EMSO-  
259 E2M3A and a discussion on the uncertainties introduced by the use of ERA5 data in computing  $\text{FCO}_2$   
260 will be presented.

### 261 3.3. Thermodynamic calculations

262 The direction and magnitude of  $\text{FCO}_2$  is governed by the difference between  $p\text{CO}_{2\text{sw}}$  and  $p\text{CO}_{2\text{atm}}$  and  
263 the air-sea  $\text{CO}_2$  gas transfer velocity (Takahashi et al., 2002):

$$265 \text{FCO}_2 = k_0 k (p\text{CO}_{2\text{sw}} - p\text{CO}_{2\text{atm}}) \quad (5)$$

266  
267 where  $k_0$  is the solubility coefficient of  $\text{CO}_2$  at in situ temperature and salinity (Weiss, 1974; Zeebe and  
268 Wolf-Gladrow, 2001) and  $k$  is the gas transfer velocity ( $\text{m day}^{-1}$ ). In this study, if the  $\text{FCO}_2 < 0$  the flux  
269 is from air to seawater, on the contrary if  $\text{FCO}_2 > 0$  the flux is from the seawater to the atmosphere.  
270 Several algorithms for  $k$  calculation exists, here the parametrization proposed by Wanninkhof (2014)  
271 was used:

$$273 k = 0.251u^2(\text{Sc}/660)^{-0.5} \quad (6)$$

274  
275 where  $u$  is the 6-hourly wind speed averages ( $\text{m s}^{-1}$ ) at 10 m height and  $\text{Sc}$  the Schmidt number for  $\text{CO}_2$ .  
276 Wanninkhof (2014), hereafter W14, has been proved to best represent the relationship between wind  
277 speed and gas exchange at a regional-to-global scale. For instance it was used in similar studies in the  
278 Mediterranean Sea (Pecci et al., 2024; Martellucci et al., 2025) and in the Adriatic basin (e.g., Urbini et  
279 al., 2020; Cantoni et al., 2024). Acknowledging that W14 provides the best fit with the Cross-Calibrated  
280 Multi-Platform (CMPP) wind product (Atlas et al., 2011), this formulation was applied using wind  
281 speed measurements from EMSO-E2M3A and from ERA5. This choice ensures methodological  
282 consistency in the comparison between  $\text{CO}_2$  flux calculated from in situ data and those from the models.  
283



284 **3.4. Thermal and non thermal component of  $p\text{CO}_{2\text{sw}}$**

285 Thermal ( $p\text{CO}_{2\text{sw}_T}$ ,  $\mu\text{atm}$ ) and non-thermal ( $p\text{CO}_{2\text{sw}_{NT}}$ ,  $\mu\text{atm}$ ) components of  $p\text{CO}_{2\text{sw}}$  were estimated  
286 according to Takahashi et al. (2002). The thermal component is associated to the effect of temperature  
287 on  $p\text{CO}_{2\text{sw}}$ , while the non-thermal component can be attributed to other factors not strictly related to  
288 temperature, as biological activity (photosynthesis and respiration), changes in dissolved inorganic  
289 carbon (DIC), mixing or advective processes and gas exchange with the atmosphere.  $p\text{CO}_{2\text{sw}_T}$  and  
290  $p\text{CO}_{2\text{sw}_{NT}}$  have been computed using the following equations:

291

$$292 \quad p\text{CO}_{2\text{sw}_T} = \text{mean}(p\text{CO}_{2\text{sw}})^{0.0423(SST_{\text{obs}} - SST_{\text{mean}})} \quad (7)$$

$$293 \quad p\text{CO}_{2\text{sw}_{NT}} = p\text{CO}_{2\text{sw}}^{0.0423(SST_{\text{mean}} - SST_{\text{obs}})} \quad (8)$$

294

295 where, *mean* refers to yearly mean values of sea surface temperature (SST, °C), while the other variables  
296 ( $p\text{CO}_{2\text{sw}}$  and  $SST_{\text{obs}}$ ) refers to the daily values measured during the study period.

297

298 **4. Results and Discussion**

299 **4.1.  $p\text{CO}_2$  dynamics and hydrography in the SAP**

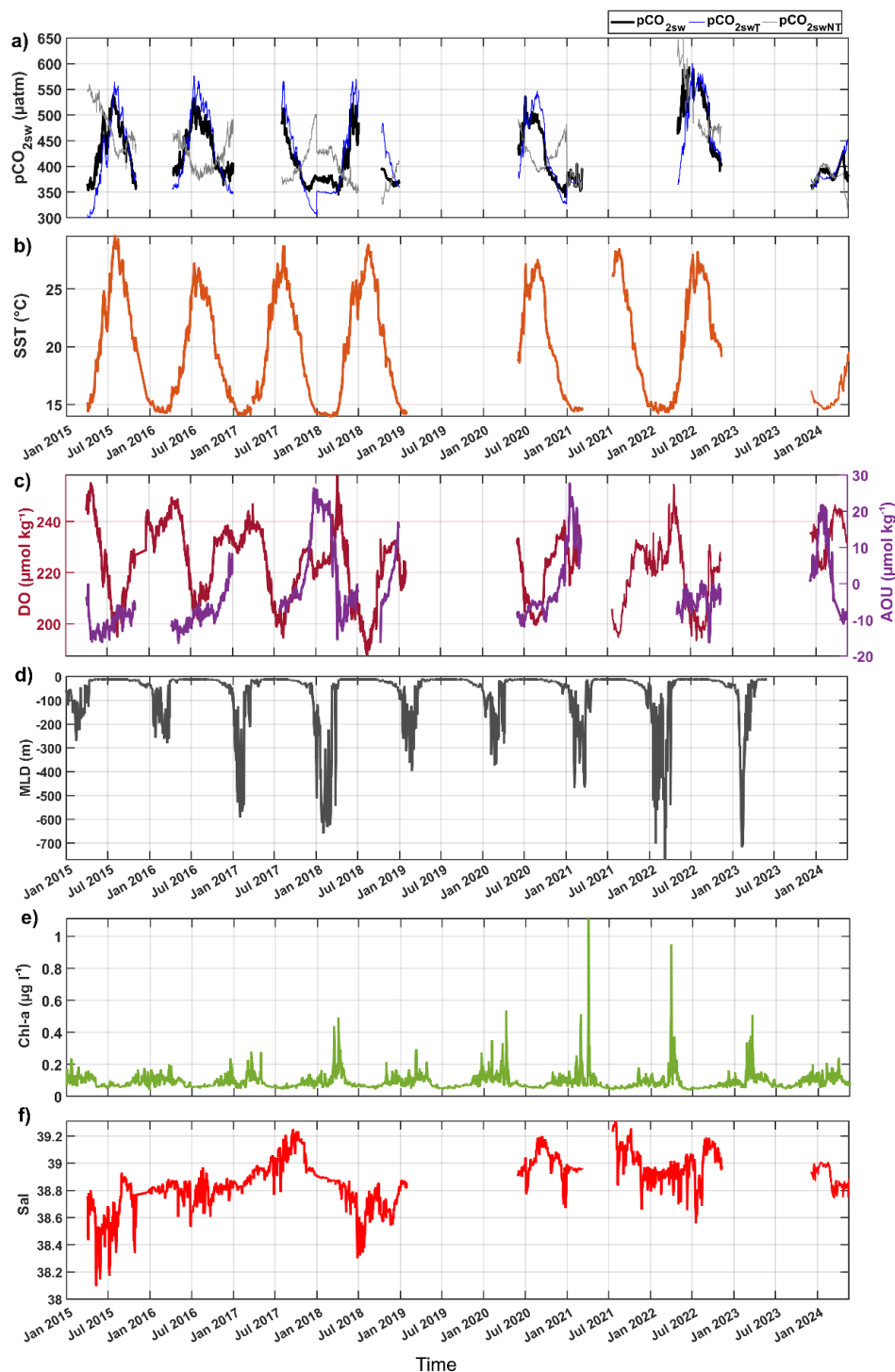
300 The time series of the daily surface  $p\text{CO}_{2\text{sw}}$  between 2015 and 2024 is presented in Fig. 2a. The  
301 incomplete coverage of the full seasonal cycle in several years, prevented a detailed assessment of  
302 interannual variability. Therefore, the discussion presented in this section mainly focuses on the  
303 seasonal patterns and its main drivers, and, when possible, on interannual differences of the seasonal  
304 cycle.

305 Mean winter values were around 380  $\mu\text{atm}$  and mean summer values reached around 484  $\mu\text{atm}$ ,  
306 resulting in a seasonal amplitude of about 100  $\mu\text{atm}$ . During winter, low sea surface temperature (SST  
307 < 15 °C; Fig. 2b) increases  $\text{CO}_2$  solubility, leading to lower  $p\text{CO}_{2\text{sw}}$ . However, during winter convection,  
308 vertical mixing increased surface  $p\text{CO}_{2\text{sw}}$ , as shown by the  $p\text{CO}_{2_{NT}}$  component (Fig. 2a). These  
309 increases were particularly evident between late December and late February of 2016–2017, 2017–  
310 2018, 2020–2021, and 2023–2024 (Fig. 2a). As described in Touratier et al. (2016) and in Inghrosso et  
311 al. (2017), vertical convection brings intermediate/deep  $\text{CO}_2$ -rich waters to the surface, causing  
312 increases in surface  $p\text{CO}_{2\text{sw}}$ . Positive AOU values during these periods (Fig. 2c) confirmed the  
313 occurrence of vertical mixing and the upward displacement of oxygen-depleted intermediate waters as  
314 described also in Martellucci et al. (2024b). The post-convection periods (usually from March to May-  
315 June) were characterised by a phytoplankton bloom (Fig. 2e), but its direct effect on  $p\text{CO}_{2\text{sw}}$  was less  
316 clear as few data were available in these periods. However, photosynthesis during the bloom, as  
317 suggested by negative AOU values and an increase in oxygen concentrations at the surface (Fig. 2c),  
318 could likely contribute to decreasing  $p\text{CO}_{2\text{sw}}$ . In spring, surface warming began, leading, in summer, to



319 maximum SST values ( $> 25\text{ }^{\circ}\text{C}$ ) and strong stratification. During this period,  $p\text{CO}_{2\text{sw}}$  reached its annual  
320 maximum, closely following the  $p\text{CO}_{2\text{sw}_T}$  component and indicating a strong thermal effect (Fig. 2a).  
321 Independent measurements from an Unmanned Surface Vehicle (USV) operating in the area in July  
322 2019 during the ATL2MED experiment (Martellucci et al., 2025) further confirmed this pattern,  
323 showing coherent short-term variations with the EMSO-E2M3A time series. Interestingly, higher  
324  $p\text{CO}_{2\text{sw}}$  values were recorded in summer 2022, with a peak in July 2022, coinciding with the occurrence  
325 of a Mediterranean Marine Heatwave (MHW). In the SAP, Pirro et al. (2024) detected positive  
326 temperature anomalies across the whole water column, with the strongest warming at the surface. Thus,  
327 the elevated  $p\text{CO}_{2\text{sw}}$  observed in this period might be linked to the MHW, although further analyses, for  
328 instance in relation to wind change patterns (e.g., Pecci et al., 2024) would be required to confirm this  
329 hypothesis. The annual cycle of surface  $p\text{CO}_{2\text{sw}}$  in the SAd was comparable to other regions of the  
330 Mediterranean Sea with generally lower values than those observed in the SAd (Dentico et al., 2025).  
331 Similar seasonal variations especially in winter were described for the northern Adriatic shelf (Ingrosso  
332 et al., 2016; Urbini et al., 2020; Cantoni et al., 2024), where intense Bora wind events and vertical  
333 mixing periodically disrupt water column stratification, promoting an efficient exchange between  
334 bottom and surface  $p\text{CO}_{2\text{sw}}$ . However, unlike the SAd, the riverine inputs in this area also play a key  
335 role in modulating the carbonate system dynamics (e.g., Giani et al., 2023). In the convective region of  
336 the northwestern Mediterranean Sea, several studies have emphasized the importance of vertical  
337 mixing, horizontal advection and biological productivity in driving  $p\text{CO}_{2\text{sw}}$  variability (e.g., Merlivat et  
338 al., 2018; Fourrier et al., 2022; Ulses et al., 2023). In the SAd the effect of biological activity was less  
339 clear because of data gaps. Nevertheless, further investigations could be essential to clarify the role of  
340 biological processes in shaping the local carbon cycle as highlighted in previous studies (Socal et al.,  
341 2012; Cerino et al., 2012). Finally, in non-convective regions such as the eastern Mediterranean Sea  
342 (Frangoulis et al., 2024), or the Lampedusa site (Pecci et al., 2024), other processes appear to control  
343  $p\text{CO}_{2\text{sw}}$  variability.

344 The analysis of hydrological data showed the highly dynamic characteristics of the region. First, the  
345 intensity and occurrence of convection in the SAd has varied substantially among years (Fig. 2d).  
346 Weaker events were recorded in 2015, 2016, 2019, and 2020, whereas deeper mixing ( $> 600\text{ m}$ )  
347 occurred in more recent years (especially after 2022). These interannual variability resulted from  
348 strong/weak air-sea interactions, where stronger heat losses could occur especially under the influence  
349 of the cold and dry Bora wind (Le Meur et al., 2025). Variations in the regional hydrographic structure,  
350 particularly changes in salinity (Amorim et al., 2024; Le Meur et al., 2025), also affected the stability  
351 of the water column and the depth of convection. This variability in salinity was associated with the  
352 inflow of Levantine/Ionian surface water, which is regulated by changes in the Northern Ionian Gyre  
353 (NIG) vorticity (Gačić et al., 2010; Rubino et al., 2020; Menna et al., 2022; Civitarese et al., 2023). The  
354 influence of NIG in the SAd was evident in the salinity measurements (Fig. 2f), which showed periods  
355 of higher salinity ( $> 39$  in 2017, 2021, 2022) and lower salinity ( $< 38.5$  in 2015, 2018).



357

358

Figure 2. Time series of daily a) Partial pressure of CO<sub>2</sub> in seawater ( $pCO_{2sw}$ ,  $\mu\text{atm}$ ) and the thermal ( $pCO_{2T}$ ,  $\mu\text{atm}$ ) and non



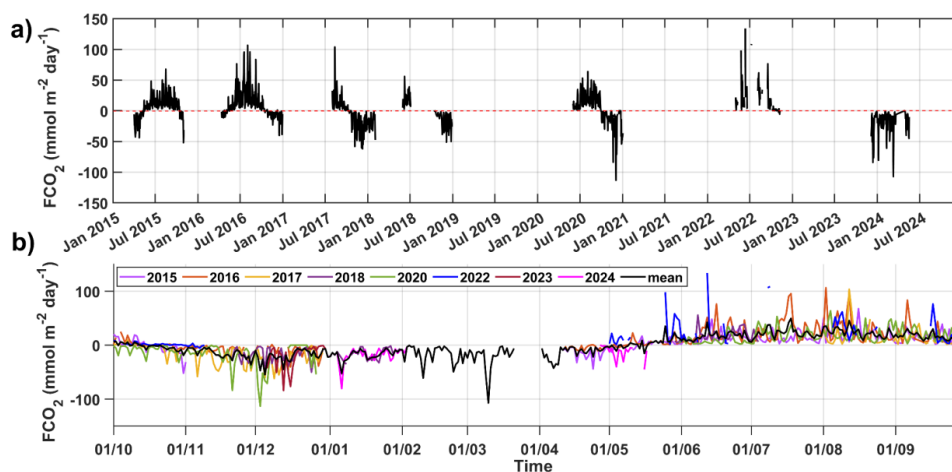
359 thermal ( $p\text{CO}_{2\text{NT}}$ ,  $\mu\text{atm}$ ) components of  $p\text{CO}_{2\text{sw}}$  ( $\mu\text{atm}$ ) in black, blue and grey, respectively; b) Sea surface temperature (SST,  $^{\circ}\text{C}$ ); c) Dissolved oxygen (DO,  $\mu\text{mol kg}^{-1}$ ) and Apparent Oxygen Utilization (AOU,  $\mu\text{mol kg}^{-1}$ ) derived from DO measured by the SBE37 ODO sensor in dark red and violet respectively; d) Mixed Layer Depth (MLD, m) from the CMEMS Mediterranean Sea Physics Reanalysis; e) Chlorophyll-a (Chl-a,  $\mu\text{g l}^{-1}$ ) used here as a proxy of primary production from the CMEMS Mediterranean Sea, Bio-Geo-Chemical, L4, monthly means, daily gapfree and climatology Satellite Observations (1997-ongoing); and f) Sea surface salinity (Sal). Time series (a, b, c and f) refers to the data measured by several instruments deployed at 2 m depth at EMSO-E2M3A between April 2015 and May 2024. Data gaps in the series were mostly due to maintenance operations and/or discarded data because they failed the quality-control procedures described in Dentico et al. (2025). Modified from Dentico et al. (2025).

368

#### 369 4.2. $\text{CO}_2$ flux: source-sink dynamics

370 Daily  $\text{FCO}_2$  in the SAd presented in this section has been computed according to Eq. (5) and Eq. (6) using as input  $p\text{CO}_{2\text{sw}}$ ,  $p\text{CO}_{2\text{atm\_E2M3Ar}}$  (Sect. 3.1) and 6-hours averaged wind speed data from EMSO-E2M3A corrected at 10 m height (Sect. 3.3).  $\text{CO}_2$  air-sea flux in the SAd presents two dominant phases: a source period, generally associated with post-convection/summer months (positive values in Fig. 3a), and a sink period, typically occurring during winter and during episodes of winter convection (negative values in Fig. 3a). While the intensity of daily values during sink and source phases exhibited high interannual variability, the timing of the transition months, i.e., the periods when the SAd shifts from a source (May) to a sink (October), occurred regularly (Fig. 3b).

378



379

380 **Figure 3.** a) Time series of daily  $\text{CO}_2$  flux ( $\text{FCO}_2$ ,  $\text{mmol m}^{-2} \text{day}^{-1}$ ) calculated with in situ measurements in the period 2015-2024 at EMSO-E2M3A; b) Daily averages of  $\text{CO}_2$  flux calculated in the different years (coloured lines) and the mean daily  $\text{FCO}_2$  ( $\text{mmol m}^{-2} \text{day}^{-1}$ ) over the entire period (2015-2024; black line). Negative flux represents  $\text{CO}_2$  influx from the air to the sea and positive flux represents  $\text{CO}_2$  outgassing from the sea to the air.

384

385 Given the observed variability (i.e., high daily variability with a regular annual cycle) and the presence  
386 of substantial data gaps in the  $\text{FCO}_2$  time series, two complementary computational approaches were



387 applied to derive robust estimates of mean CO<sub>2</sub> fluxes in the SAP over the past decade. By considering  
 388 two different orders in the process of aggregating data for computing averages, the sensitivity of data  
 389 sampling irregularity to the overall mean was verified. In the first approach (hereafter M1), the daily  
 390 means for each day of the year were calculated. Outliners were then identified and removed through  
 391 visual inspection, with particular attention to values not supported by a sufficiently large number of  
 392 observations. Finally, monthly means were derived, and the overall mean for the entire study period  
 393 (2015-2024) was computed from the 12 monthly averages. In the second approach (hereafter M2), a  
 394 2015-2024 time series of the monthly values is computed for those months with at least 14 valid daily  
 395 values. The mean over the full period was subsequently obtained from these monthly values. A  
 396 summary of the monthly means obtained with M1 and M2 is reported in Table 2.

397

398 **Table 2.** Monthly mean of FCO<sub>2</sub> (mmol m<sup>-2</sup> day<sup>-1</sup>) in the SAd calculated with in situ data from the EMSO-E2M3A regional  
 399 facility in the period 2015-2024 using two different computation methods. Relative difference was calculated as M1 - M2  
 400 divided by M1.

Month of the year	M1 (mmol m <sup>-2</sup> day <sup>-1</sup> )	M2 (mmol m <sup>-2</sup> day <sup>-1</sup> )	M1 - M2	Relative difference
January	-17.92	-17.89	-0.04	0.0020
February	-16.75	-15.96	-0.78	0.0469
March	-12.79	-12.79	0.00	0.0000
April	-14.26	-11.02	-3.23	0.2269
May	6.36	9.80	-3.44	-0.5410
June	16.67	16.31	0.36	0.0215
July	22.49	21.06	1.43	0.0635
August	24.11	22.90	1.22	0.0504
September	15.61	15.58	0.03	0.0017
October	-1.99	-1.88	-0.11	0.0577
November	-15.30	-15.62	0.32	-0.0209
December	-20.14	-19.69	-0.45	0.0222

401

402 Both methods produced consistent results, with an average difference of approximately 5 % between  
 403 M1 and M2. The largest discrepancies between the two methods occurred in April and May. In April  
 404 these can be due to the lower data availability (Fig. 3b), as only two years of data were available. On  
 405 the contrary, in May a transition between source and sink conditions occurs, thus explaining the larger  
 406 differences between M1 and M2. Similarly, in February, data for only one year (2024) was available  
 407 throughout the month with the addition of a few days at the beginning of February 2018 making this



408 approach not robust enough to have reliable results (higher difference between M1 and M2). Finally, in  
409 March data were available only in 2024, and the proposed aggregating processes produced no difference  
410 between M1 and M2. Notwithstanding these potential limitations derived by data availability, the results  
411 indicated that, over the last decade, the SAd has functioned predominantly as a moderate carbon sink.  
412 For the period 2015-2024, mean  $FCO_2$  values ranged from  $-1.15 \text{ mmol m}^{-2} \text{ day}^{-1}$  (M1) to  $-0.76 \text{ mmol}$   
413  $\text{m}^{-2} \text{ day}^{-1}$  (M2). Although modest in magnitude, these values consistently pointed to a net  $CO_2$  uptake,  
414 underscoring the potential role of the SAd in regional carbon sequestration, as suggested by Ingrassio et  
415 al. (2017). Further, these results confirm the role of dense water formation sites as primary drivers of  
416 carbon sequestration. Indeed, the northern Adriatic Sea has been reported to act as an effective  $CO_2$  sink  
417 during winter, spring, and autumn, with mean daily fluxes of about  $-2.9 \text{ mmol m}^{-2} \text{ day}^{-1}$  (Catalano et  
418 al., 2014; Cantoni et al., 2024). In the Gulf of Lion, Ulses et al. (2023) showed that the area functions  
419 as a net  $CO_2$  sink on an annual scale, with an estimated carbon sequestration rate of approximately -  
420  $1.29 \text{ mmol m}^{-2} \text{ day}^{-1}$  (estimated mean was  $-0.47 \text{ mol C m}^{-2} \text{ year}^{-1}$ ).

421

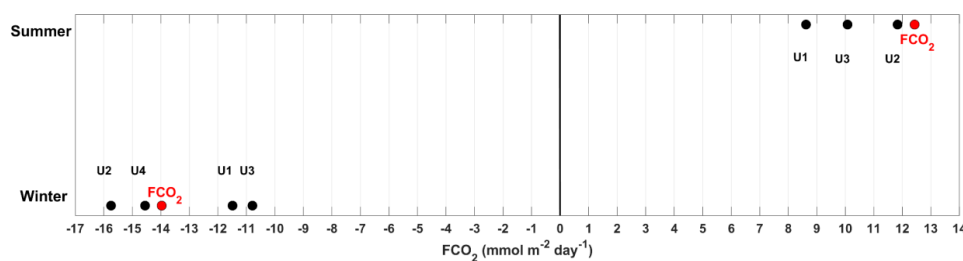
#### 422 **4.3 Estimated uncertainties in $FCO_2$**

423 The accuracy of the  $CO_2$  flux estimates presented in this study was influenced by several systematic  
424 sources of uncertainty, arising from the type of data used to compute the two relevant parts of the W14  
425 formula, i.e., the the gas transfer velocity  $k$  and the difference between  $pCO_{2sw}$  and  $pCO_{2atm}$  ( $\Delta CO_2$ ).

426 To assess the source of uncertainty related to  $k$ , three different wind datasets were used to compute  $CO_2$   
427 flux other than the one used in Sec. 4.2. These considerations are particularly relevant given the presence  
428 of temporal gaps in the time series presented here. The first case (hereafter U1) considered the  
429 conversion applied to EMSO-E2M3A wind speed data from 2 m to 10 m height (see Sec. 3.3). The  
430 second case (hereafter U2) accounted for the effect of a different temporal resolution considering a daily  
431 average of the wind data directly calculated from hourly observation without performing 6-hourly  
432 means. The use of 6-hourly wind speed averages is widely adopted as it smooths extreme values,  
433 reduces noise in buoy data, better represents the slow air–sea  $CO_2$  exchange, and ensures consistency  
434 with model outputs. The third case (hereafter U3) used wind data from ERA5. Considering U3 is  
435 particularly relevant especially when in situ measurements are unavailable, and model-derived data  
436 must be integrated. Moreover, given that RD uses the same W14 formula and ERA5 wind data, the  
437 assessment of U3 can be used to help disentangling model errors that derive from the air-sea flux  
438 calculation (e.g., different wind products) from those derived from the  $\Delta CO_2$  discrepancies. Uncertainty  
439 in each of the three cases was quantified as the mean difference between fluxes calculated using the  
440 reference condition (10 m in situ wind speed averaged every 6 hours) and the alternative inputs (2 m  
441 height and 6 hours average in situ wind speed, for U1; daily average of 10 m height in situ wind speed,  
442 for U2; and 10 m height and 6 hours average ERA5 wind speed, for U3). For the  $\Delta CO_2$ , the systematic  
443 uncertainty associated with the use of  $pCO_{2atm}$  derived using  $xCO_2$  from Lampedusa site (Sec. 3.1) was  
444 considered. This latter, hereafter referred to as U4, was estimated by comparing winter fluxes calculated



445 with the uncorrected  $p\text{CO}_{2\text{atm}}$  to those calculated after adding  $+2.67 \mu\text{atm}$  to the  $p\text{CO}_{2\text{atm}}$  time series  
 446 (Sec. 3.1). All the uncertainties, except U4, were computed separately for two extended seasonal  
 447 regimes: the summer/source period (from April to September) and the winter/sink period (from October  
 448 to March). U4 was restricted to the winter period only as the offset of  $+2.67 \mu\text{atm}$  was computed  
 449 considering winter months only (December to March, Sec. 3.1). A summary of the results is shown in  
 450 Fig. 4.  
 451



452

453 **Figure 4.** Summary of the different sources of uncertainties (U1, U2, U3, U4) considered in the study associated with the  
 454 estimated  $\text{FCO}_2$  ( $\text{mmol m}^{-2} \text{day}^{-1}$ ) in the SAAd ( $\text{FCO}_2$  in red) in the period 2015-2024 calculated as described in Sec. 4.2. Winter  
 455 includes the months from October to March and summer includes the months from April to September.  
 456

457 The different sources of uncertainty influenced  $\text{FCO}_2$  estimates in different ways across seasons. The  
 458 largest seasonal differences were observed for U1 and U3, whereas U2 showed lower variability  
 459 between winter and summer. Among the three, U2 contributed the least to the overall uncertainty  
 460 especially during summer, suggesting that the choice between using daily mean calculated from 6-  
 461 hourly means or daily average calculated from hourly observations (without performing 6-hourly  
 462 means) wind speed had only a minor effect on the final  $\text{FCO}_2$  estimates. However, this choice appeared  
 463 to have a higher influence during winter. The effect of using wind speed data at a lower height than the  
 464 standard 10 m height (U1), as proposed in W14, has already been discussed (e.g., Griessbaum et al.,  
 465 2010; Nickford et al., 2022; Nickford et al., 2024). The authors have shown that wind speed measured  
 466 closer to the air–sea exchange interface could better represent the local forcing, particularly under  
 467 conditions of high atmospheric stratification. Such measurements may also capture transient  
 468 phenomena, including gusts and micro-turbulence, and could improve our understanding of the role of  
 469 wave breaking and bubble-mediated transfer in modulating the  $\text{CO}_2$  flux. While these aspects are  
 470 beyond the scope of the present study, they highlighted the value of further investigations into near-  
 471 surface wind dynamics for the estimation of  $\text{FCO}_2$ . U3 showed the largest differences with respect to  
 472  $\text{FCO}_2$  estimated as described in Sec. 4.2, underscoring potential limitations in using ERA5 reanalysis  
 473 data as a reliable regional proxy for local wind speed conditions. A more detailed analysis (Fig. S4, S5,  
 474 Supplementary Material) revealed high differences between the wind speed measured at EMSO-  
 475 E2M3A and ERA5 especially in high Beaufort scale wind (<https://www.rmets.org/metmatters/beaufort->



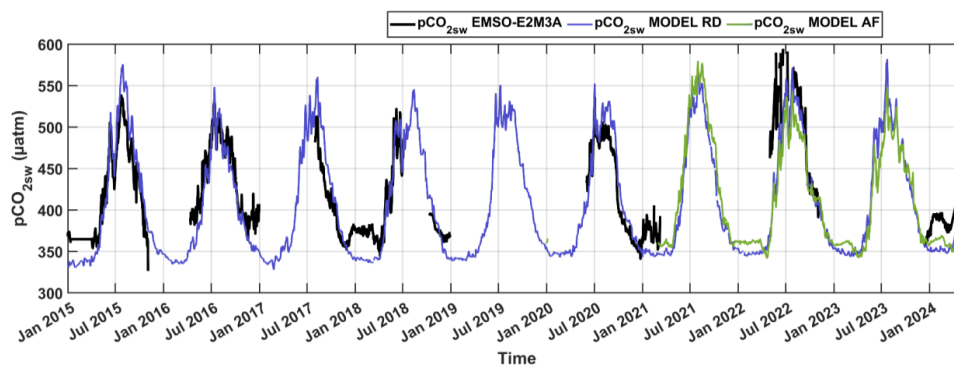
476 wind-scale). Given the quadratic dependence of  $k$  on wind speed, as a result, the choice of the wind  
477 speed field used is expected to lead to changes in  $\text{FCO}_2$  as emphasized by Takahashi et al. (2002).  
478 Considering the uncertainty of the  $\Delta\text{CO}_2$  components, errors associated with corrected or not corrected  
479  $p\text{CO}_{2\text{atm}}$  in the SAD were negligible. Finally, it is important to mention that in respect to  $\Delta\text{CO}_2$  the error  
480 related to the use of in situ sensor-based  $p\text{CO}_{2\text{sw}}$  as input for  $\text{FCO}_2$  should also be computed. Sensor-  
481 based  $p\text{CO}_{2\text{sw}}$  not always met the manufacturer and the ICOS or SOCAT accuracies (Steinhoff et al.,  
482 2025). As shown in Dentico et al., (2025) the measured values by Pro-Oceanus membrane sensor can  
483 report higher ( $>10 \mu\text{atm}$ ) differences with  $p\text{CO}_{2\text{sw}}$  calculated from discrete seawater samples. Here, it  
484 was not possible to compute a statistically robust measure of this uncertainty. This was due to the very  
485 low number of discrete seawater samples and the bias of their temporal distribution (Dentico et al.,  
486 2025). Most of the available  $p\text{CO}_{2\text{sw}}$  from discrete seawater samples were collected in October and not  
487 only failed to adequately represent the full seasonal cycle of  $\text{CO}_2$ . Additionally, October was the month  
488 that showed the transition from the positive to negative phases possibly emphasizing differences in  
489  $\text{FCO}_2$  calculation. While the random component of uncertainty can be quantified for  $p\text{CO}_{2\text{sw}}$  (e.g., using  
490 standard bootstrapping approaches based on the manufacturer-specified precision of the  $p\text{CO}_{2\text{sw}}$  sensor),  
491 the focus here was on the potentially systematic sources of uncertainty in the computation of  $\text{FCO}_2$ .  
492 This choice reflected the substantial effort involved in assembling multiple source dataset.

493

#### 494 **4.4. $p\text{CO}_{2\text{sw}}$ and $\text{FCO}_2$ : in situ data and model comparison**

495 The in situ  $p\text{CO}_{2\text{sw}}$  and physical data proved to be a reliable asset for model validation, thus a  
496 comparison between the RD and AF CMEMS products for  $p\text{CO}_{2\text{sw}}$  and  $\text{FCO}_2$  was computed. The  
497 comparison between daily  $p\text{CO}_{2\text{sw}}$  from CMEMS (Sect. 2) and  $p\text{CO}_{2\text{sw}}$  measured by the probe for a  
498 decade-long period highlighted a coherent temporal evolution (Fig. 5). A RMSE of  $35.96 \mu\text{atm}$  and a  
499 significant correlation coefficient of 0.82 ( $p \text{ value} < 0.01$ ) between the two datasets was found.  
500 Nevertheless, during summer, model data were on average higher than  $p\text{CO}_{2\text{sw}}$  from the probe, with a  
501 mean difference between RD and the probe data of  $+34.22 \mu\text{atm}$ . The only exception was in 2022, when  
502  $p\text{CO}_{2\text{sw}}$  from the probe was higher than CMEMS data (both RD and AF). On the contrary, in winter RD  
503 data were on average lower than the probe, with a mean difference between the two datasets of  $-26.87$   
504  $\mu\text{atm}$ . This can be explained by the increase in the  $p\text{CO}_{2\text{sw}}$  shown by probe data between late December  
505 and late February that was not resolved by the model, which underestimated it by approximately  $45$   
506  $\mu\text{atm}$ . Finally, in autumn and spring the mean differences were smaller ( $+5.13 \mu\text{atm}$  and  $-16.12 \mu\text{atm}$ ,  
507 respectively). By contrast, with lower intensity, the AF product was able to capture this increase (Fig.  
508 5). Similarly to RD, also AF was not able to consistently reproduce the higher  $p\text{CO}_{2\text{sw}}$  values measured  
509 by the probe in summer 2022.

510

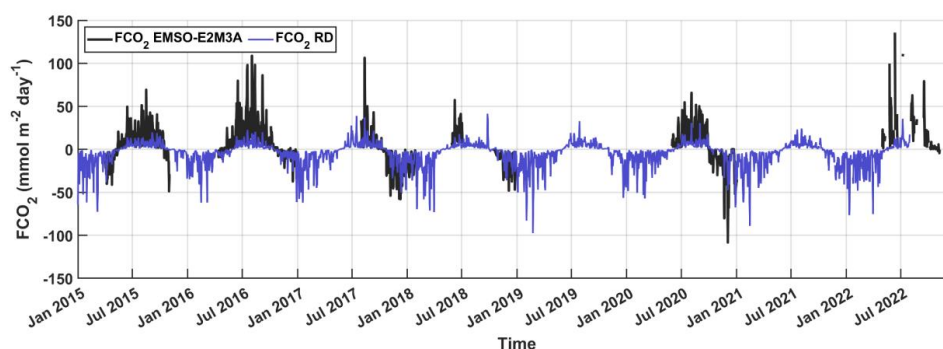


511  
 512 **Figure 5.** Time series of daily  $p\text{CO}_{2\text{sw}}$  ( $\mu\text{atm}$ ) measured at the EMSO-E2M3A regional observatory in black,  $p\text{CO}_{2\text{sw}}$  ( $\mu\text{atm}$ )  
 513 from the Mediterranean Sea Biogeochemistry Reanalysis (RD) in blue and the Mediterranean Sea Biogeochemistry Analysis  
 514 and Forecast (AF) in green. RD data after July 2022 were integrated with the interim reanalysis.

515

516 The comparison between  $\text{FCO}_2$  derived from in situ data and from the model is presented in Fig. 6.  
 517 Both datasets consistently capture the two main seasonal phases of the region, with a source period  
 518 during summer and a sink period during winter. However, notable differences in absolute values  
 519 emerged, particularly in summer. A main factor in these differences was related to the  $p\text{CO}_{2\text{sw}}$   
 520 measurements as discussed in the previous section. Additionally, in both seasons, the different wind  
 521 forcing used by the model (ERA5) could also be a contributing factor of the  $\text{FCO}_2$  difference (see Sect.  
 522 4.3 and Fig. S5, Supplementary Material). On the contrary, the difference between model and in situ  
 523 temperature and/or salinity was not considered a driving factor of the in situ and RD  $\text{FCO}_2$  difference  
 524 (Fig. S6, Supplementary Material). Nevertheless, an RMSE of  $16.89 \text{ mmol m}^{-2} \text{ day}^{-1}$  with a correlation  
 525 coefficient of 0.89 ( $p \text{ value} < 0.01$ ) was calculated between  $\text{FCO}_2$  from RD and  $\text{FCO}_2$  derived from  
 526 observational data.

527



528  
 529 **Figure 6.** Time series of daily  $\text{FCO}_2$  ( $\text{mmol m}^{-2} \text{ day}^{-1}$ ) calculated with in situ data measured at the EMSO-E2M3A and  $\text{FCO}_2$   
 530 ( $\text{mmol m}^{-2} \text{ day}^{-1}$ ) from the Mediterranean Sea Biogeochemistry Reanalysis (RD) represented by the black and violet curves  
 531 respectively. Model data after July 2022 were integrated with the interim reanalysis.



532

533 Considering the relatively good performance of the RD, and the temporal bias in the in situ FCO<sub>2</sub> time  
534 series (e.g., the winter periods were by far undersampled with respect to summer periods), the use of  
535 the CMEMS RD product to compute the overall FCO<sub>2</sub> average filling the gaps of the in situ data was  
536 tested. A bias (B) of the CMEMS RD was calculated as the difference between the mean flux over the  
537 entire period (2015-2024) and the mean flux considering only the days with observations. B was then  
538 added to the mean flux calculated with in situ observations, resulting in -4.9 mmol m<sup>-2</sup> day<sup>-1</sup> and -4.5  
539 mmol m<sup>-2</sup> day<sup>-1</sup>, respectively for the two M1 and M2 methods. Even if these estimations should be  
540 considered with caution, they further confirm that the southern Adriatic acted as a moderate carbon sink  
541 over the last decade.

542

## 543 **5. Conclusion**

544 A time series of  $p\text{CO}_{2\text{sw}}$  and hydrography from autonomous sensors over the past 10 years were  
545 analyzed to characterize  $p\text{CO}_{2\text{sw}}$  and carbon flux in the dense water formation site of the southern  
546 Adriatic Sea. The data were collected by several sensors deployed at the EMSO-E2M3A South Adriatic  
547 regional facility and ICOS ERIC observatory (nominal position 41.5053°N, 18.0806°E) which is  
548 located in the central and deepest part of the SAd, the SAP. Surface  $p\text{CO}_{2\text{sw}}$  dynamics were  
549 characterized by strong seasonal fluctuations, with a difference of 100  $\mu\text{atm}$  between winter and  
550 summer. In winter, average  $p\text{CO}_{2\text{sw}}$  were around 380  $\mu\text{atm}$ , with marked increase especially during  
551 wintertime convection periods when CO<sub>2</sub>-rich intermediate and deep water were upwelled to the  
552 surface. In summer, average values increased up to around 500  $\mu\text{atm}$  driven by higher sea surface  
553 temperatures. The effect of biological processes was difficult to identify due to lower availability of  
554 data during post-convection/bloom periods. CO<sub>2</sub> fluxes were characterized by two distinct regimes of  
555 post-convection/summer CO<sub>2</sub> released to the atmosphere (mean summer month/source flux of +12.43  
556 mmol m<sup>-2</sup> day<sup>-1</sup>) and convection/winter CO<sub>2</sub> ocean uptake (mean winter months/sink flux of -15.82  
557 mmol m<sup>-2</sup> day<sup>-1</sup>). One of the key results of this study was to demonstrate that over the past decade the  
558 SAd acted as a moderate carbon sink. Two different orders of aggregating the data for computing  
559 decadal averages were used due to the sampling irregularity. These calculations resulted in a mean sink  
560 flux of -1.15 mmol m<sup>-2</sup> day<sup>-1</sup> (M1) and -0.76 mmol m<sup>-2</sup> day<sup>-1</sup> (M2) in the period 2015-2024. Several  
561 sources of systematic uncertainty associated with the two most relevant parts of the flux formula, i.e.,  
562 the gas transfer velocity ( $k$ ) and  $\Delta\text{CO}_2$ , were also quantified. For  $k$ , the selection of the wind forcing to  
563 be used in FCO<sub>2</sub> calculation is one of the primary sources of uncertainties. Particularly, the correction  
564 applied to convert in situ wind speed data from 2 m height to 10 m height and the use of ERA5 dataset  
565 as input variable for the calculation of FCO<sub>2</sub>. Thus, careful consideration must be given to both the wind  
566 product selected and the height at which wind is measured or modeled, particularly in coastal areas or  
567 under high-wind conditions where gas exchange may be over- or underestimated (Nickford et al., 2024).



568 Furthermore, as many oceanic areas lack in situ wind observations, model-derived wind products (e.g.,  
569 ERA5, CCMP) are frequently used. Assessing the reliability and limitations of these datasets is  
570 therefore critical for improving flux estimates in data-sparse regions. Regarding  $\Delta\text{CO}_2$ , the use of  
571  $p\text{CO}_{2\text{atm}}$  from another location appeared to have a minor influence on the final  $\text{FCO}_2$ . While in this study  
572 the focus was on systematic uncertainty, the  $p\text{CO}_{2\text{sw}}$  one was not estimated due to the lack of discrete  
573 seawater samples. By proving to be an important asset for model validation, the  $p\text{CO}_{2\text{sw}}$  and  
574 hydrographic time series allowed to quantify existing specific discrepancies in the regional CMEMS  
575 model product such as a lack in winter  $p\text{CO}_{2\text{sw}}$  increase, and over/underestimation of the seasonal  
576 amplitude. Nevertheless, the integration of model and observational data further confirms that the SAD  
577 was a site of moderate atmospheric  $\text{CO}_2$  sink in the last decade.

578 The SAD, as many other regions in the Mediterranean Sea, is currently undergoing profound physical  
579 changes, including increasing sea surface temperature, rising salinity, and the potential intensification  
580 of extreme events. These trends are likely to affect convection intensity and timing, with potential  
581 consequences for carbon dynamics in the basin on a climatic scale. In this context, the long-term  
582 monitoring carried out in the region, by combining sustained in situ observations with modeling  
583 approaches, are necessary to fully understand the complex interplay between physical forcing,  
584 biogeochemical processes, and carbon dynamics in the context of climate change.

585

#### 586 **Data availability**

587 The in situ data used in this study are freely accessible at the National Oceanographic Data Center  
588 (NODC) of the National Institute of Oceanography and Applied Geophysics  
589 (<https://doi.org/10.13120/y2hw-1j63>; Cardin et al., 2025). Model data are also publicly available  
590 through the Copernicus Marine Service website following the links provided in the manuscript.

591

#### 592 **Team list:**

593 Carlotta Dentico, Gianpiero Cossarini, Giuseppe Civitarese, Michele Giani, Angelo Rubino and  
594 Vanessa Cardin.

595

#### 596 **Author contribution:**

597 CD: data curation, investigation, validation, writing (original draft), writing (review and editing),  
598 conceptualisation, formal analysis. GCos: investigation, writing (review and editing), conceptualisation.  
599 GCiv: investigation, writing (review and editing), conceptualisation. MG: investigation, writing (review  
600 and editing), conceptualisation. AR: investigation, writing (review and editing), conceptualisation. VC:  
601 funding acquisition, project administration, investigation, writing (review and editing),  
602 conceptualisation, supervision.

603



604 **Competing interest:**

605 The authors declare that they have no conflict of interest.

606

607 **Acknowledgements:**

608 This work benefited from access to the E2M3A South Adriatic Regional Facility, an EMSO-IT/ICOS-  
609 IT site operated by OGS. This study has been conducted using E.U. Copernicus Marine Service  
610 Information. The authors are very grateful to the OGS technical and biogeochemical teams, as well as  
611 the CNR-ISP for their essential contributions and continued efforts in operating and maintaining the  
612 EMSO/ICOS-E2M3A regional facility. The authors also acknowledge ChatGPT creators as it was used  
613 to improve the English writing in some parts of this manuscript.

614

615 **Financial support:** The dataset used and the related activities were partially funded by the EMSO  
616 Italian Joint Research Unit, OGS, and the EU Next Generation EU programme (Mission 4, Component  
617 2, Investment 3.1: “Fund for the realisation of an integrated system of research and innovation  
618 infrastructures”) under Project IR0000032 – ITINERIS (Italian Integrated Environmental Research  
619 Infrastructures System). Additional support for  $p\text{CO}_2$  instruments data acquisition and calibration was  
620 also provided by ICOS.

621

622 **References**

623

624 Amitai, Y., Ashkenazy, Y., and Gildor, H.: The Effect of the Source of Deep Water in the Eastern Mediterranean  
625 on Western Mediterranean Intermediate and Deep Water, *Front. Mar. Sci.*, 7, 615975,  
626 <https://doi.org/10.3389/fmars.2020.615975>, 2021.

627 Amorim, F. L. L., Le Meur, J., Wirth, A., and Cardin, V.: Tipping of the double-diffusive regime in the southern  
628 Adriatic Pit in 2017 in connection with record high-salinity values, *Ocean Sci.*, 20, 463–474,  
629 <https://doi.org/10.5194/os-20-463-2024>, 2024.

630 Atlas, R., Hoffman, R. N., Ardizzone, J., Leidner, S. M., Jusem, J. C., Smith, D. K., and Gombos, D.: A Cross-  
631 calibrated, Multiplatform Ocean Surface Wind Velocity Product for Meteorological and Oceanographic  
632 Applications, *Bull. Amer. Meteor. Soc.*, 92, 157–174, <https://doi.org/10.1175/2010BAMS2946.1>, 2011.

633 Agustí-Panareda, A., Barré, J., Massart, S., Inness, A., Aben, I., Ades, M., Baier, B. C., Balsamo, G., Borsdorff,  
634 T., Bousserez, N., Boussetta, S., Buchwitz, M., Cantarello, L., Crevoisier, C., Engelen, R., Eskes, H., Flemming,  
635 J., Garrigues, S., Hasekamp, O., Huijnen, V., Jones, L., Kipling, Z., Langerock, B., McNorton, J., Meilhac, N.,  
636 Noël, S., Parrington, M., Peuch, V.-H., Ramonet, M., Razinger, M., Reuter, M., Ribas, R., Suttie, M., Sweeney,  
637 C., Tarniewicz, J., and Wu, L.: Technical note: The CAMS greenhouse gas reanalysis from 2003 to 2020, *Atmos.*  
638 *Chem. Phys.*, 23, 3829–3859, <https://doi.org/10.5194/acp-23-3829-2023>, 2023.

639 Bakker, D. C., Alin, S. R., Bates, N. R., Becker, M., Feely, R. A., and Gritzalis, T. (2023). SOCAT version 2023–  
640 An alarming decline in the ocean CO<sub>2</sub> observing capacity.



- 641 Benson, B. B. and Krause, D.: The concentration and isotopic fractionation of oxygen dissolved in freshwater and  
642 seawater in equilibrium with the atmosphere<sup>1</sup>, *Limnology & Oceanography*, 29, 620–632,  
643 <https://doi.org/10.4319/lo.1984.29.3.0620>, 1984.
- 644 Bignami, F., Salusti, E., and Schiarini, S.: Observations on a bottom vein of dense water in the southern Adriatic  
645 and Ionian seas, *J. Geophys. Res.*, 95, 7249–7259, <https://doi.org/10.1029/JC095iC05p07249>, 1990.
- 646 Cantoni, C., Luchetta, A., Chiggiato, J., Cozzi, S., Schroeder, K., and Langone, L.: Dense water flow and  
647 carbonate system in the southern Adriatic: A focus on the 2012 event, *Marine Geology*, 375, 15–27,  
648 <https://doi.org/10.1016/j.margeo.2015.08.013>, 2016.
- 649 Cantoni, C., De Vittor, C., Faganeli, J., Giani, M., Kovač, N., Malej, A., Ogrinc, N., Tamše, S., and Turk, V.:  
650 Carbonate system and acidification of the Adriatic Sea, *Marine Chemistry*, 267, 104462,  
651 <https://doi.org/10.1016/j.marchem.2024.104462>, 2024.
- 652 Cardin, V., Bensi, M., and Pacciaroni, M.: Variability of water mass properties in the last two decades in the South  
653 Adriatic Sea with emphasis on the period 2006–2009, *Continental Shelf Research*, 31, 951–965,  
654 <https://doi.org/10.1016/j.csr.2011.03.002>, 2011.
- 655 Cardin, V., Le Meur, J., Ursella, L., Dentico, C., Siena, G., Mansutti, P., Brunetti, F., and Partescano, E.: EMSO-  
656 E2M3A-B-Surface-time-series-South-Adriatic [dataset], <https://doi.org/10.13120/y2hw-1j63>, 2025a.
- 657 Cardin, V., Dentico, C., Brunetti, F., Bubbi, A., Chiaruttini, L., Civitarese, G., Comici, C., Corbo, A., Gerin, R.,  
658 Giani, M., Kuchler, S., Le Meur, J., Mansutti, P., Savonitto, G. and Siena, G.: EMSO-E2M3A-B-Surface-time-  
659 series-South-Adriatic [dataset], <https://doi.org/10.13120/y2hw-1j63>, 2025b.
- 660 Catalano, G., Azzaro, M., Bastianini, M., Bellucci, L. G., Bernardi Aubry, F., Bianchi, F., Burca, M., Cantoni, C.,  
661 Caruso, G., Casotti, R., Cozzi, S., Del Negro, P., Fonda Umami, S., Giani, M., Giuliani, S., Kovacevic, V., La  
662 Ferla, R., Langone, L., Luchetta, A., Monticelli, L. S., Piacentino, S., Pugnetti, A., Ravaoli, M., Socal, G.,  
663 Spagnoli, F., and Ursella, L.: The carbon budget in the northern Adriatic Sea, a winter case study, *JGR*  
664 *Biogeosciences*, 119, 1399–1417, <https://doi.org/10.1002/2013JG002559>, 2014.
- 665 Cerino, F., Bernardi Aubry, F., Coppola, J., La Ferla, R., Maimone, G., Socal, G., and Totti, C.: Spatial and  
666 temporal variability of pico-, nano- and microphytoplankton in the offshore waters of the southern Adriatic Sea  
667 (Mediterranean Sea), *Continental Shelf Research*, 44, 94–105, <https://doi.org/10.1016/j.csr.2011.06.006>, 2012.
- 668 Chiggiato, J., Bergamasco, A., Borghini, M., Falcieri, F. M., Falco, P., Langone, L., Miserocchi, S., Russo, A.,  
669 and Schroeder, K.: Dense-water bottom currents in the Southern Adriatic Sea in spring 2012, *Marine Geology*,  
670 375, 134–145, <https://doi.org/10.1016/j.margeo.2015.09.005>, 2016.
- 671 Civitarese, G., Gačić, M., Lipizer, M., and Eusebi Borzelli, G. L.: On the impact of the Bimodal Oscillating  
672 System (BiOS) on the biogeochemistry and biology of the Adriatic and Ionian Seas (Eastern Mediterranean),  
673 *Biogeosciences*, 7, 3987–3997, <https://doi.org/10.5194/bg-7-3987-2010>, 2010.
- 674 Civitarese, G., Gačić, M., Batistić, M., Bensi, M., Cardin, V., Dulčić, J., Garić, R., and Menna, M.: The BiOS  
675 mechanism: History, theory, implications, *Progress in Oceanography*, 216, 103056,  
676 <https://doi.org/10.1016/j.pocean.2023.103056>, 2023.



- 677 Cossarini, G., Feudale, L., Teruzzi, A., Bolzon, G., Coidessa, G., Solidoro, C., Di Biagio, V., Amadio, C., Lazzari,  
678 P., Brosich, A., and Salon, S.: High-Resolution Reanalysis of the Mediterranean Sea Biogeochemistry (1999–  
679 2019), *Front. Mar. Sci.*, 8, 741486, <https://doi.org/10.3389/fmars.2021.741486>, 2021.
- 680 Doney, S. C., Fabry, V. J., Feely, R. A., and Kleypas, J. A.: Ocean Acidification: The Other CO<sub>2</sub> Problem, *Annu.*  
681 *Rev. Mar. Sci.*, 1, 169–192, <https://doi.org/10.1146/annurev.marine.010908.163834>, 2009.
- 682 Escudier, R., Clementi, E., Cipollone, A., Pistoia, J., Drudi, M., Grandi, A., Lyubartsev, V., Lecci, R., Aydogdu,  
683 A., Delrosso, D., Omar, M., Masina, S., Coppini, G., and Pinardi, N.: A High Resolution Reanalysis for the  
684 Mediterranean Sea, *Front. Earth Sci.*, 9, 702285, <https://doi.org/10.3389/feart.2021.702285>, 2021.
- 685 Fourier, M., Coppola, L., D’Ortenzio, F., Migon, C., and Gattuso, J.: Impact of Intermittent Convection in the  
686 Northwestern Mediterranean Sea on Oxygen Content, Nutrients, and the Carbonate System, *JGR Oceans*, 127,  
687 e2022JC018615, <https://doi.org/10.1029/2022JC018615>, 2022.
- 688 Frangoulis, C., Stamatakis, N., Pettas, M., Michelinakis, S., King, A. L., Giannoudi, L., Tsiaras, K., Christodoulaki,  
689 S., Seppälä, J., Thyssen, M., Borges, A. V., and Krasakopoulou, E.: A carbonate system time series in the Eastern  
690 Mediterranean Sea. Two years of high-frequency in-situ observations and remote sensing, *Front. Mar. Sci.*, 11,  
691 1348161, <https://doi.org/10.3389/fmars.2024.1348161>, 2024.
- 692 Friedlingstein, P., O’Sullivan, M., Jones, M. W., Andrew, R. M., Hauck, J., Landschützer, P., Le Quéré, C., Li,  
693 H., Luijckx, I. T., Olsen, A., Peters, G. P., Peters, W., Pongratz, J., Schwingshackl, C., Sitch, S., Canadell, J. G.,  
694 Ciais, P., Jackson, R. B., Alin, S. R., Arneeth, A., Arora, V., Bates, N. R., Becker, M., Bellouin, N., Berghoff, C.  
695 F., Bittig, H. C., Bopp, L., Cadule, P., Campbell, K., Chamberlain, M. A., Chandra, N., Chevallier, F., Chini, L.  
696 P., Colligan, T., Decayeux, J., Djeutchouang, L. M., Dou, X., Duran Rojas, C., Enyo, K., Evans, W., Fay, A. R.,  
697 Feely, R. A., Ford, D. J., Foster, A., Gasser, T., Gehlen, M., Gkritzalis, T., Grassi, G., Gregor, L., Gruber, N.,  
698 Gürses, Ö., Harris, I., Hefner, M., Heinke, J., Hurtt, G. C., Iida, Y., Ilyina, T., Jacobson, A. R., Jain, A. K.,  
699 Jarníková, T., Jersild, A., Jiang, F., Jin, Z., Kato, E., Keeling, R. F., Klein Goldewijk, K., Knauer, J., Korsbakken,  
700 J. I., Lan, X., Lauvset, S. K., Lefèvre, N., Liu, Z., Liu, J., Ma, L., Maksyutov, S., Marland, G., Mayot, N., McGuire,  
701 P. C., Metzl, N., Monacci, N. M., Morgan, E. J., Nakaoka, S.-I., Neill, C., Niwa, Y., Nützel, T., Olivier, L., Ono,  
702 T., Palmer, P. I., Pierrot, D., Qin, Z., Resplandy, L., Roobaert, A., Rosan, T. M., Rödenbeck, C., Schwinger, J.,  
703 Smallman, T. L., Smith, S. M., Sospedra-Alfonso, R., Steinhoff, T., et al.: Global Carbon Budget 2024, *Earth*  
704 *Syst. Sci. Data*, 17, 965–1039, <https://doi.org/10.5194/essd-17-965-2025>, 2025.
- 705 Gattuso, J-P, and Hansson L. (Eds). Ocean acidification. Oxford university press, 2011
- 706 Gačić, M., Civitarese, G., Miserochi, S., Cardin, V., Crise, A., and Mauri, E.: The open-ocean convection in the  
707 Southern Adriatic: a controlling mechanism of the spring phytoplankton bloom, *Continental Shelf Research*, 22,  
708 1897–1908, [https://doi.org/10.1016/S0278-4343\(02\)00050-X](https://doi.org/10.1016/S0278-4343(02)00050-X), 2002.
- 709 Gačić, M., Borzelli, G. L. E., Civitarese, G., Cardin, V., and Yari, S.: Can internal processes sustain reversals of  
710 the ocean upper circulation? The Ionian Sea example, *Geophysical Research Letters*, 37, 2010GL043216,  
711 <https://doi.org/10.1029/2010GL043216>, 2010.
- 712 Garcia, H. E. and Gordon, L. I.: Oxygen solubility in seawater: Better fitting equations, *Limnol. Oceanogr.*, 37,  
713 1307–1312, <https://doi.org/10.4319/lo.1992.37.6.1307>, 1992.



- 714 García-Ibáñez, M. I., Gualart, E. F., Lucas, A., Pascual, J., Gasol, J. M., Marrasé, C., Calvo, E., and Pelejero, C.:  
715 Two new coastal time-series of seawater carbonate system variables in the NW Mediterranean Sea: rates and  
716 mechanisms controlling pH changes, *Front. Mar. Sci.*, 11, 1348133, <https://doi.org/10.3389/fmars.2024.1348133>,  
717 2024.
- 718 Giani, M., Ogrinc, N., Tamše, S., and Cozzi, S.: Elevated River Inputs of the Total Alkalinity and Dissolved  
719 Inorganic Carbon in the Northern Adriatic Sea, *Water*, 15, 894, <https://doi.org/10.3390/w15050894>, 2023.
- 720 Griessbaum, F., Moat, B. I., Narita, Y., Yelland, M. J., Klemm, O., and Uematsu, M.: Uncertainties in wind speed  
721 dependent CO<sub>2</sub> transfer velocities due to airflow distortion at anemometer sites on ships, *Atmos. Chem. Phys.*, 10,  
722 5123–5133, <https://doi.org/10.5194/acp-10-5123-2010>, 2010.
- 723 Gruber, N., Bakker, D. C. E., DeVries, T., Gregor, L., Hauck, J., Landschützer, P., McKinley, G. A., and Müller,  
724 J. D.: Trends and variability in the ocean carbon sink, *Nat Rev Earth Environ*, 4, 119–134,  
725 <https://doi.org/10.1038/s43017-022-00381-x>, 2023.
- 726 Hassoun, A. E. R., Fakhri, M., Raad, N., Abboud-Abi Saab, M., Gemayel, E., and De Carlo, E. H.: The carbonate  
727 system of the Eastern-most Mediterranean Sea, Levantine Sub-basin: Variations and drivers, *Deep Sea Research*  
728 *Part II: Topical Studies in Oceanography*, 164, 54–73, <https://doi.org/10.1016/j.dsr2.2019.03.008>, 2019.
- 729 Hassoun, A. E. R., Bantelman, A., Canu, D., Comeau, S., Galdies, C., Gattuso, J.-P., Giani, M., Grelaud, M.,  
730 Hendriks, I. E., Ibello, V., Idrissi, M., Krasakopoulou, E., Shaltout, N., Solidoro, C., Swarzenski, P. W., and  
731 Ziveri, P.: Ocean acidification research in the Mediterranean Sea: Status, trends and next steps, *Front. Mar. Sci.*,  
732 9, 892670, <https://doi.org/10.3389/fmars.2022.892670>, 2022.
- 733 Hersbach, H., Bell, B., Berrisford, P., Biavati, G., Horányi, A., Muñoz Sabater, J., Nicolas, J., Peubey, C., Radu,  
734 R., Rozum, I., Schepers, D., Simmons, A., Soci, C., Dee, D., Thépaut, J.-N.: ERA5 hourly data on single levels  
735 from 1940 to present. Copernicus Climate Change Service (C3S) Climate Data Store (CDS), [dataset],  
736 <https://doi.org/10.24381/cds.adbb2d47>, 2023.
- 737 Ilyina, T., Zeebe, R. E., Maier-Reimer, E., and Heinze, C.: Early detection of ocean acidification effects on marine  
738 calcification, *Global Biogeochemical Cycles*, 23, 2008GB003278, <https://doi.org/10.1029/2008GB003278>, 2009.
- 739 Ingrosso, G., Giani, M., Comici, C., Kralj, M., Piacentino, S., De Vittor, C., and Del Negro, P.: Drivers of the  
740 carbonate system seasonal variations in a Mediterranean gulf, *Estuarine, Coastal and Shelf Science*, 168, 58–70,  
741 <https://doi.org/10.1016/j.ecss.2015.11.001>, 2016.
- 742 Ingrosso, G., Bensi, M., Cardin, V., and Giani, M.: Anthropogenic CO<sub>2</sub> in a dense water formation area of the  
743 Mediterranean Sea, *Deep Sea Research Part I: Oceanographic Research Papers*, 123, 118–128,  
744 <https://doi.org/10.1016/j.dsr.2017.04.004>, 2017.
- 745 Intergovernmental Panel On Climate Change (Ipcc): Climate Change 2021 – The Physical Science Basis: Working  
746 Group I Contribution to the Sixth Assessment Report of the Intergovernmental Panel on Climate Change, 1st ed.,  
747 Cambridge University Press, <https://doi.org/10.1017/9781009157896>, 2023.
- 748 Kapsenberg, L., Alliouane, S., Gazeau, F., Mousseau, L., and Gattuso, J.-P.: Coastal ocean acidification and  
749 increasing total alkalinity in the northwestern Mediterranean Sea, *Ocean Sci.*, 13, 411–426,  
750 <https://doi.org/10.5194/os-13-411-2017>, 2017.



- 751 Lan, X., Tans, P. and K.W. Thoning: Trends in globally-averaged CO<sub>2</sub> determined from NOAA Global  
752 Monitoring Laboratory measurements. Version Friday, 05-Dec-2025 11:36:40 MST:  
753 <https://gml.noaa.gov/ccgg/trends/global.html>, last access: 16 December 2025.
- 754 Laruelle, G. G., Cai, W.-J., Hu, X., Gruber, N., Mackenzie, F. T., and Regnier, P.: Continental shelves as a variable  
755 but increasing global sink for atmospheric carbon dioxide, *Nat Commun*, 9, 454, <https://doi.org/10.1038/s41467-017-02738-z>, 2018.
- 757 Le Meur, J., Wirth, A., Paladini De Mendoza, F., Miserocchi, S., and Cardin, V.: Intermittent supply of dense  
758 water to the deep South Adriatic Pit: an observational study, *Front. Mar. Sci.*, 12, 1516780,  
759 <https://doi.org/10.3389/fmars.2025.1516780>, 2025.
- 760 Le Traon, P. Y., Reppucci, A., Alvarez Fanjul, E., Aouf, L., Behrens, A., Belmonte, M., Bentamy, A., Bertino,  
761 L., Brando, V. E., Kreiner, M. B., Benkiran, M., Carval, T., Ciliberti, S. A., Claustre, H., Clementi, E., Coppini,  
762 G., Cossarini, G., De Alfonso Alonso-Muñoyerro, M., Delamarche, A., Dibarboure, G., Dinessen, F., Drevillon,  
763 M., Drillet, Y., Faugere, Y., Fernández, V., Fleming, A., Garcia-Hermosa, M. I., Sotillo, M. G., Garric, G.,  
764 Gasparin, F., Giordan, C., Gehlen, M., Gregoire, M. L., Guinehut, S., Hamon, M., Harris, C., Hernandez, F.,  
765 Hinkler, J. B., Hoyer, J., Karvonen, J., Kay, S., King, R., Lavergne, T., Lemieux-Dudon, B., Lima, L., Mao, C.,  
766 Martin, M. J., Masina, S., Melet, A., Buongiorno Nardelli, B., Nolan, G., Pascual, A., Pistoia, J., Palazov, A.,  
767 Piolle, J. F., Pujol, M. I., Pequignet, A. C., Peneva, E., Pérez Gómez, B., Petit De La Villeon, L., Pinardi, N.,  
768 Pisano, A., Pouliquen, S., Reid, R., Remy, E., Santoleri, R., Siddorn, J., She, J., Staneva, J., Stoffelen, A., Tonani,  
769 M., Vandenbulcke, L., Von Schuckmann, K., Volpe, G., Wettre, C., and Zacharioudaki, A.: From Observation to  
770 Information and Users: The Copernicus Marine Service Perspective, *Front. Mar. Sci.*, 6, 234,  
771 <https://doi.org/10.3389/fmars.2019.00234>, 2019.
- 772 Lee, K., Sabine, C. L., Tanhua, T., Kim, T.-W., Feely, R. A., and Kim, H.-C.: Roles of marginal seas in absorbing  
773 and storing fossil fuel CO<sub>2</sub>, *Energy Environ. Sci.*, 4, 1133, <https://doi.org/10.1039/c0ee00663g>, 2011.
- 774 Lohbeck, K. T., Riebesell, U., and Reusch, T. B. H.: Adaptive evolution of a key phytoplankton species to ocean  
775 acidification, *Nature Geosci.*, 5, 346–351, <https://doi.org/10.1038/ngeo1441>, 2012.
- 776 Malanotte-Rizzoli, P.: The Northern Adriatic Sea as a Prototype of Convection and Water Mass Formation on the  
777 Continental Shelf, in: *Elsevier Oceanography Series*, vol. 57, Elsevier, 229–239, [https://doi.org/10.1016/S0422-9894\(08\)70070-9](https://doi.org/10.1016/S0422-9894(08)70070-9), 1991.
- 779 Mantziafou, A. and Lascaratos, A.: An eddy resolving numerical study of the general circulation and deep-water  
780 formation in the Adriatic Sea, *Deep Sea Research Part I: Oceanographic Research Papers*, 51, 921–952,  
781 <https://doi.org/10.1016/j.dsr.2004.03.006>, 2004.
- 782 Martellucci, R., Giani, M., Mauri, E., Coppola, L., Paulsen, M., Fourier, M., Pensieri, S., Cardin, V., Dentico,  
783 C., Bozzano, R., Cantoni, C., Lucchetta, A., Izquierdo, A., Bruno, M., and Skjelvan, I.: CO<sub>2</sub> and hydrography  
784 acquired by autonomous surface vehicles from the Atlantic Ocean to the Mediterranean Sea: data correction and  
785 validation, *Earth Syst. Sci. Data*, 16, 5333–5356, <https://doi.org/10.5194/essd-16-5333-2024>, 2024a.
- 786 Martellucci, R., Menna, M., Mauri, E., Pirro, A., Gerin, R., Paladini De Mendoza, F., Garić, R., Batistić, M., Di  
787 Biagio, V., Giordano, P., Langone, L., Miserocchi, S., Gallo, A., Notarstefano, G., Savonitto, G., Bussani, A.,  
788 Pacciaroni, M., Zuppelli, P., and Poulain, P.-M.: Recent changes of the dissolved oxygen distribution in the deep



- 789 convection cell of the southern Adriatic Sea, *Journal of Marine Systems*, 245, 103988,  
790 <https://doi.org/10.1016/j.jmarsys.2024.103988>, 2024b.
- 791 Martellucci, R., Dentico, C., Coppola, L., Skjelvan, I., Giani, M., Pensieri, S., Cantoni, C., Cardin, V., Fourier,  
792 M., Bozzano, R., Paulsen, M., and Mauri, E.: Air-sea CO<sub>2</sub> exchange in the Eastern Atlantic and the Mediterranean  
793 Sea based on autonomous surface measurements, *Front. Mar. Sci.*, 12, 1633617,  
794 <https://doi.org/10.3389/fmars.2025.1633617>, 2025.
- 795 Marullo, S., Pitarch, J., Bellacicco, M., Sarra, A. G. D., Meloni, D., Monteleone, F., Sferlazzo, D., Artale, V., and  
796 Santoleri, R.: Air–Sea Interaction in the Central Mediterranean Sea: Assessment of Reanalysis and Satellite  
797 Observations, *Remote Sensing*, 13, 2188, <https://doi.org/10.3390/rs13112188>, 2021.
- 798 Menna, M., Martellucci, R., Notarstefano, G., Mauri, E., Gerin, R., Pacciaroni, M., Bussani, A., Pirro, A., Poulain,  
799 P-M.: Record-breaking high salinity in the South Adriatic Pit in 2020, in: Copernicus Ocean State Report, issue  
800 6. *Journal of Operational Oceanography*, 15(sup1), 1–220. <https://doi.org/10.1080/1755876X.2022.2095169>,  
801 2022.
- 802 Merlivat, L., Boutin, J., Antoine, D., Beaumont, L., Golbol, M., and Vellucci, V.: Increase of dissolved inorganic  
803 carbon and decrease in pH in near-surface waters in the Mediterranean Sea during the past two decades,  
804 *Biogeosciences*, 15, 5653–5662, <https://doi.org/10.5194/bg-15-5653-2018>, 2018.
- 805 Meyer, J. and Riebesell, U.: Reviews and Syntheses: Responses of coccolithophores to ocean acidification: a  
806 meta-analysis, *Biogeosciences*, 12, 1671–1682, <https://doi.org/10.5194/bg-12-1671-2015>, 2015.
- 807 Nickford, S., Palter, J. B., Donohue, K., Fassbender, A. J., Gray, A. R., Long, J., Sutton, A. J., Bates, N. R., and  
808 Takeshita, Y.: Autonomous Wintertime Observations of Air-Sea Exchange in the Gulf Stream Reveal a Perfect  
809 Storm for Ocean CO<sub>2</sub> Uptake, *Geophysical Research Letters*, 49, e2021GL096805,  
810 <https://doi.org/10.1029/2021GL096805>, 2022.
- 811 Nickford, S., Palter, J. B., and Mu, L.: The Importance of Contemporaneous Wind and *p*CO<sub>2</sub> Measurements for  
812 Regional Air-Sea CO<sub>2</sub> Flux Estimates, *JGR Oceans*, 129, e2023JC020744,  
813 <https://doi.org/10.1029/2023JC020744>, 2024.
- 814 Ovchinnikov, I. M., Zats, V. I., Krivosheya, V. G., & Udodov, A. I.: Formation of deep Eastern Mediterranean  
815 waters in the Adriatic Sea. *Oceanology*, 25(6), 704–707, 1985.
- 816 Park, J., Stock, C. A., Yang, X., Dunne, J. P., Rosati, A., John, J., and Zhang, S.: Modeling Global Ocean  
817 Biogeochemistry With Physical Data Assimilation: A Pragmatic Solution to the Equatorial Instability, *J Adv*  
818 *Model Earth Syst*, 10, 891–906, <https://doi.org/10.1002/2017MS001223>, 2018.
- 819 Pecci, M., Sferlazzo, D., Anello, F., Becagli, S., Colella, S., Silvestri, L. D., Iorio, T. D., Meloni, D., Monteleone,  
820 F., Piacentino, S., Principato, E., and Sarra, A. D.: Large influence of the 2022–23 marine heatwave on the air-sea  
821 CO<sub>2</sub> flux in the Central Mediterranean, <https://doi.org/10.22541/essoar.173393985.55347710/v1>, 11 December  
822 2024.
- 823 Peixoto, J.P. and Oort, A.H.: *Physics of Climate*. American Institute of Physics, New York.  
824 <https://doi.org/10.1063/1.2809772>, 1992.



- 825 Pirro, A., Martellucci, R., Gallo, A., Kubin, E., Mauri, E., Juza, M., Notarstefano, G., Pacciaroni, M., Bussani,  
826 A., and Menna, M.: Subsurface warming derived from Argo floats during the 2022 Mediterranean marine heat  
827 wave, *State Planet*, 4-osr8, 1–12, <https://doi.org/10.5194/sp-4-osr8-18-2024>, 2024.
- 828 Ravaoli, M., Bergami, C., Riminucci, F., Langone, L., Cardin, V., Di Sarra, A., Aracri, S., Bastianini, M., Bensi,  
829 M., Bergamasco, A., Bommarito, C., Borghini, M., Bortoluzzi, G., Bozzano, R., Cantoni, C., Chiggiato, J., Crisafi,  
830 E., D'Adamo, R., Durante, S., Fanara, C., Grilli, F., Lipizer, M., Marini, M., Miserocchi, S., Paschini, E., Penna,  
831 P., Pensieri, S., Pugnetti, A., Raicich, F., Schroeder, K., Siena, G., Specchiulli, A., Stanghellini, G., Vetranò, A.,  
832 and Crise, A.: The RITMARE Italian Fixed-Point Observatory Network (IFON) for marine environmental  
833 monitoring: a case study, *Journal of Operational Oceanography*, 9, s202–s214,  
834 <https://doi.org/10.1080/1755876X.2015.1114806>, 2016.
- 835 Resplandy, L., Hogikyan, A., Müller, J. D., Najjar, R. G., Bange, H. W., Bianchi, D., Weber, T., Cai, W. -J.,  
836 Doney, S. C., Fennel, K., Gehlen, M., Hauck, J., Lacroix, F., Landschützer, P., Le Quéré, C., Roobaert, A.,  
837 Schwinger, J., Berthet, S., Bopp, L., Chau, T. T. T., Dai, M., Gruber, N., Ilyina, T., Kock, A., Manizza, M.,  
838 Lachkar, Z., Laruelle, G. G., Liao, E., Lima, I. D., Nissen, C., Rödenbeck, C., Séférian, R., Toyama, K., Tsujino,  
839 H., and Regnier, P.: A Synthesis of Global Coastal Ocean Greenhouse Gas Fluxes, *Global Biogeochemical Cycles*,  
840 38, e2023GB007803, <https://doi.org/10.1029/2023GB007803>, 2024.
- 841 Robinson, A. R., Leslie, W. G., Theocharis, A., and Lascaratos, A.: Mediterranean Sea Circulation, in:  
842 *Encyclopedia of Ocean Sciences*, Elsevier, 1689–1705, <https://doi.org/10.1006/rwos.2001.0376>, 2001.
- 843 Roether, W. and Schlitzer, R.: Eastern Mediterranean deep water renewal on the basis of chlorofluoromethane  
844 and tritium data, *Dynamics of Atmospheres and Oceans*, 15, 333–354, [https://doi.org/10.1016/0377-0265\(91\)90025-B](https://doi.org/10.1016/0377-0265(91)90025-B), 1991.
- 846 Roobaert, A., Resplandy, L., Laruelle, G. G., Liao, E., and Regnier, P.: Unraveling the Physical and Biological  
847 Controls of the Global Coastal CO<sub>2</sub> Sink, *Global Biogeochemical Cycles*, 38, e2023GB007799,  
848 <https://doi.org/10.1029/2023GB007799>, 2024.
- 849 Rubino, A., Gačić, M., Bensi, M., Kovačević, V., Malačić, V., Menna, M., Negretti, M. E., Sommeria, J.,  
850 Zanchettin, D., Barreto, R. V., Ursella, L., Cardin, V., Civitarese, G., Orlić, M., Petelin, B., and Siena, G.:  
851 Experimental evidence of long-term oceanic circulation reversals without wind influence in the North Ionian Sea,  
852 *Sci Rep*, 10, 1905, <https://doi.org/10.1038/s41598-020-57862-6>, 2020.
- 853 Salon, S., Cossarini, G., Bolzon, G., Feudale, L., Lazzari, P., Teruzzi, A., Solidoro, C., and Crise, A.: Novel  
854 metrics based on Biogeochemical Argo data to improve the model uncertainty evaluation of the CMEMS  
855 Mediterranean marine ecosystem forecasts, *Ocean Sci.*, 15, 997–1022, <https://doi.org/10.5194/os-15-997-2019>,  
856 2019.
- 857 di Sarra, A., Di Iorio, T., Piacentino, S., and Sferlazzo, D.: ICOS ATC NRT CO<sub>2</sub> growing time series from  
858 Lampedusa (8.0 m), 2025-04-01–2025-10-19, ICOS RI, [dataset],  
859 [https://hdl.handle.net/11676/jZB47zujZMJcR\\_HI5CtLEVHD](https://hdl.handle.net/11676/jZB47zujZMJcR_HI5CtLEVHD), 2025.
- 860 Schlitzer, R., Roether, W., Oster, H., Junghans, H.-G., Hausmann, M., Johannsen, H., and Michelato, A.:  
861 Chlorofluoromethane and oxygen in the Eastern Mediterranean, *Deep Sea Research Part A. Oceanographic*  
862 *Research Papers*, 38, 1531–1551, [https://doi.org/10.1016/0198-0149\(91\)90088-W](https://doi.org/10.1016/0198-0149(91)90088-W), 1991.



- 863 Schroeder, K., and Chiggiato J. (Eds): Oceanography of the Mediterranean Sea: An introductory guide. Elsevier,  
864 2022.
- 865 Takahashi, T., Sutherland, S. C., Sweeney, C., Poisson, A., Metzl, N., Tilbrook, B., Bates, N., Wanninkhof, R.,  
866 Feely, R. A., Sabine, C., Olafsson, J., and Nojiri, Y.: Global sea–air CO<sub>2</sub> flux based on climatological surface  
867 ocean pCO<sub>2</sub>, and seasonal biological and temperature effects, Deep Sea Research Part II: Topical Studies in  
868 Oceanography, 49, 1601–1622, [https://doi.org/10.1016/S0967-0645\(02\)00003-6](https://doi.org/10.1016/S0967-0645(02)00003-6), 2002.
- 869 Touratier, F., Goyet, C., Houpert, L., De Madron, X. D., Lefèvre, D., Stabholz, M., and Guglielmi, V.: Role of  
870 deep convection on anthropogenic CO<sub>2</sub> sequestration in the Gulf of Lions (northwestern Mediterranean Sea),  
871 Deep Sea Research Part I: Oceanographic Research Papers, 113, 33–48, <https://doi.org/10.1016/j.dsr.2016.04.003>,  
872 2016.
- 873 Turchetto, M., Boldrin, A., Langone, L., and Miserocchi, S.: Physical and biogeochemical processes controlling  
874 particle fluxes variability and carbon export in the Southern Adriatic, Continental Shelf Research, 44, 72–82,  
875 <https://doi.org/10.1016/j.csr.2011.05.005>, 2012a.
- 876 Turchetto, M., Boldrin, A., Langone, L., and Miserocchi, S.: Physical and biogeochemical processes controlling  
877 particle fluxes variability and carbon export in the Southern Adriatic, Continental Shelf Research, 44, 72–82,  
878 <https://doi.org/10.1016/j.csr.2011.05.005>, 2012b.
- 879 Ulses, C., Estournel, C., Marsaleix, P., Soetaert, K., Fourrier, M., Coppola, L., Lefèvre, D., Touratier, F., Goyet,  
880 C., Guglielmi, V., Kessouri, F., Testor, P., and Durrieu De Madron, X.: Seasonal dynamics and annual budget of  
881 dissolved inorganic carbon in the northwestern Mediterranean deep-convection region, Biogeosciences, 20, 4683–  
882 4710, <https://doi.org/10.5194/bg-20-4683-2023>, 2023.
- 883 Urbini, L., Inghrosso, G., Djakovac, T., Piacentino, S., and Giani, M.: Temporal and Spatial Variability of the CO<sub>2</sub>  
884 System in a Riverine Influenced Area of the Mediterranean Sea, the Northern Adriatic, Front. Mar. Sci., 7, 679,  
885 <https://doi.org/10.3389/fmars.2020.00679>, 2020.
- 886 Vilibić, I. and Supić, N.: Dense water generation on a shelf: the case of the Adriatic Sea, Ocean Dynamics, 55,  
887 403–415, <https://doi.org/10.1007/s10236-005-0030-5>, 2005.
- 888 Volpe, G., Colella, S., Brando, V. E., Forneris, V., La Padula, F., Di Cicco, A., Sammartino, M., Bracaglia, M.,  
889 Artuso, F., and Santoleri, R.: Mediterranean ocean colour Level 3 operational multi-sensor processing, Ocean  
890 Sci., 15, 127–146, <https://doi.org/10.5194/os-15-127-2019>, 2019.
- 891 Wanninkhof, R.: Relationship between wind speed and gas exchange over the ocean revisited, Limnology &  
892 Ocean Methods, 12, 351–362, <https://doi.org/10.4319/lom.2014.12.351>, 2014.
- 893 Weiss, R. F.: Carbon dioxide in water and seawater: the solubility of a non-ideal gas, Marine Chemistry, 2, 203–  
894 215, [https://doi.org/10.1016/0304-4203\(74\)90015-2](https://doi.org/10.1016/0304-4203(74)90015-2), 1974.
- 895 Weiss, R. F. and Price, B. A.: Nitrous oxide solubility in water and seawater, Marine Chemistry, 8, 347–359,  
896 [https://doi.org/10.1016/0304-4203\(80\)90024-9](https://doi.org/10.1016/0304-4203(80)90024-9), 1980.  
897
- 898 Zeebe, R. E. and Wolf-Gladrow, D.: CO<sub>2</sub> in seawater: equilibrium, kinetics, isotopes, in: Elsevier Oceanography  
899 Series, vol. 65, edited by: Halpem, D., Elsevier B.V., Amsterdam, the Netherlands, 2001.